AFIT/GA/ENY/97D-04

EFFECTS OF LIQUID TRANSPIRATION COOLING

ON HEAT TRANSFER TO THE DIVERGING

REGION OF A POROUS-WALLED NOZZLE

THESIS

Daniel J. Schieb, B.S.

AFIT/GA/ENY/97D-04

19980210 029

Disclaimer Statement

The views expressed in this thesis are those of the author and do not reflect the official policy or position of the Department of Defense or the U. S. Government.

AFIT/GA/ENY/97D-04

EFFECTS OF LIQUID TRANSPIRATION COOLING

ON HEAT TRANSFER TO THE DIVERGING

REGION OF A POROUS-WALLED NOZZLE

THESIS

Presented to the Faculty of the Graduate School of Engineering

of the Air Force Institute of Technology

Air University

In Partial Fulfillment of the

Requirements for the Degree of

Master of Science in Astronautical Engineering
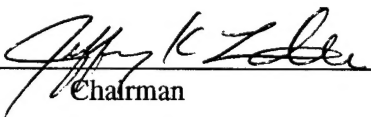
Daniel J. Schieb, B.S.
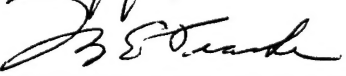
Captain, USAF

December 1997

EFFECTS OF LIQUID TRANSPIRATION COOLING

ON HEAT TRANSFER TO THE DIVERGING

REGION OF A POROUS-WALLED NOZZLE

Daniel J. Schieb, B.S.
Captain, USAF

Approved:

_____
Chairman

_____

_____

26 Nov 97
date

26 Nov 97
date

26 Nov 97
date

Preface

This research is the continuation of a long series of cooling studies performed in the AFIT Low Pressure Shock Tube, from film cooling of flat plates to transpiration cooling of porous nozzle throat walls. There are two significant advances made in this study. First, the use of the AFIT High Pressure Shock Tube allows the study of much higher stagnation pressures and temperatures. Second, choosing a liquid over a gas as the cooling agent not only enhances the insulating properties of the boundary layer, but also introduces the evaporation process to absorb additional energy.

Daniel J. Schieb

Table of Contents

List of Figures

List of Tables

List of Symbols

Symbol	Description	Units
A	Area	m^2
c	Specific Heat	J/kg K
D	Diameter	m
D_{AB}	Binary Mass Diffusion Coefficient	m^2/s
E	Voltage	μV
h	Convection Heat Transfer Coefficient	W/m^2 K
h_{fg}	Latent Heat of Vaporization	J/kg
h_m	Convection Mass Transfer Coefficient	m/s
k	Thermal Conductivity	W/m K
L	Characteristic Length	m
M	Mach Number	(dimensionless)
Nu_L	Nusselt Number (hL/k_f)	(dimensionless)
n"	Mass Flux	kg/s m^2
P	Pressure	Pa
Pr	Prandtl Number ($c_p\mu/k$)	(dimensionless)
q"	Heat Flux	W/m^2
Re_L	Reynolds Number ($\rho VL/\mu$)	(dimensionless)
r	Recovery Factor	(dimensionless)
r_c	Nozzle Throat Radius of Curvature	m
T	Temperature	K
t	Time	s
V	Velocity	m/s
x	Distance into Substrate	m
y	Distance from the Wall Surface in the Normal Direction	m
α	Thermal Diffusivity ($k/\rho c_p$)	m^2/s
γ	Ratio of Specific Heats (c_p/c_v)	(dimensionless)
ε	Emissivity	(dimensionless)

η	Nondimensional Parameter $(x/(4\alpha t)^{0.5})$ *or* Cooling Effectiveness(dimensionless) *or* %	
μ	Dynamic Viscosity	Ns/m^2
ρ	Density	kg/m^3
π	Pi = 3.1416	(dimensionless)
σ	Stefan-Boltzman Constant = 5.67×10^{-8}	$W/m^2\,K^4$

Subscripts

1	Shock Tunnel Fluid Property of the Initial Driven Gas
5	Shock Tunnel Fluid Property Behind the Reflected Shock
o	Stagnation Condition
A	Species A – Coolant
aw	Adiabatic Wall
bl	Boundary Layer
c	Cooled
conv	Convection
d	Dry
evap	Evaporation
f	Fluid
g	Primary Gas
i	Initial Value $(t \le 0)$
p	Constant Pressure
rad	Radiation
s	Surface
t	Nozzle Throat
u	Uncooled
w	Wall Surface *or* Wet
∞	Freestream Gas Property

Abstract

This research effort investigated the effects of evaporation of water on the heat transferred to the wall of the diverging portion of a porous walled nozzle. The experiment was performed using the AFIT High Pressure Shock Tube configured with a two-dimensional Mach 3 nozzle. One flat surface of the nozzle was fitted with a layer of porous stainless steel from the nozzle throat to the exit. Surface temperature data were taken in this region using fast-response coaxial thermocouples. Knowledge of the thermodynamic properties of the thermocouple material and the surface temperature history allowed the determination of the surface heat transfer. Data were taken with a dry nozzle as a control, and then again with the porous material saturated with water. Results for the control were validated using empirical relations. Data were taken for stagnation pressures ranging from 2.0 to 5.2 MPa. The effectiveness of the liquid transpiration cooling was found to decrease with increasing stagnation conditions. Reduction in heat transfer coefficient ranged from 130% at a stagnation pressure of 2.0 MPa to only 10% at stagnation pressures between 3.0 and 5.2 MPa. This type of cooling demonstrated outstanding potential for low pressure applications, but may not be effective at the high stagnation conditions needed for advanced rocket performance.

EFFECTS OF LIQUID TRANSPIRATION COOLING

ON HEAT TRANSFER TO THE DIVERGING

REGION OF A POROUS-WALLED NOZZLE

I. Introduction

1.1 Background

Currently, the primary method of cooling rocket nozzles is regenerative cooling, where cryogenic fuels are pumped through channels within the nozzle wall before entering the combustion chamber. This method has been employed for decades and is well understood. In recent years, however, the need for more powerful launch vehicles has arisen. One major limiting factor for modern rocket performance is the thermal limitation of the nozzle material. This limitation is now driving the need for thorough research of supplemental (or even replacement) methods of nozzle cooling before significant increases in thrust chamber pressures and temperatures can be achieved.

One type of cooling that has been studied for years is film cooling, which employs injection ports through which a relatively cool gas is injected into the flow to enhance the insulating effects of the boundary layer. It requires relatively large injection mass flow per unit area, which can cause thrust losses due to disturbance of the primary flow (Lenertz, 1994:1). Transpiration cooling is essentially the limiting case of film cooling, involving the injection of a gas or liquid through a porous material over a relatively large surface area. This type of cooling has demonstrated the ability to achieve the same success as film cooling, but with significantly lower injection flow rates (Lenertz, 1994: 48). An additional benefit of transpiration cooling is

that it has little to no effect on nozzle performance in terms of specific impulse (Keener, 1994: 66).

Liquid transpiration cooling simply implies the use of a liquid cooling agent rather than a gas. This study proposes to demonstrate liquid transpiration cooling to have the same cooling success as gas transpiration cooling, with the added benefit of the evaporation process to absorb additional energy.

1.2 Problem Statement

With regenerative cooling, the hot gas exhausted through the nozzle transfers heat to the nozzle wall by convection and radiation. The heat then flows through the nozzle wall by conduction and is transferred by convection to the coolant, where it is carried away. (see Fig 1.1)
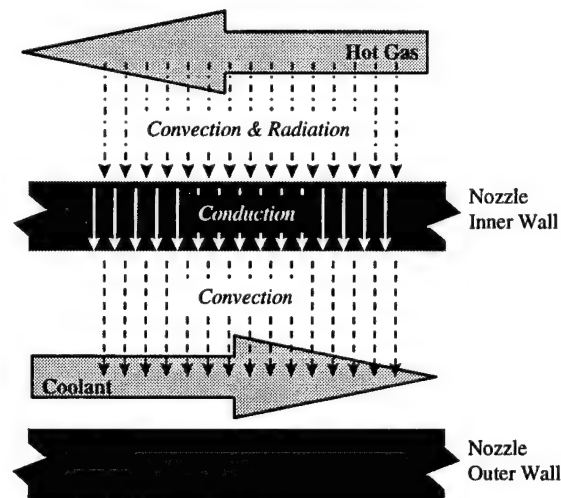

Figure 1.1 Schematic of Regenerative Cooling

The temperature of the nozzle inner wall reaches steady state when the heat transferred in from the hot gas balances the heat transferred out to the coolant. With higher performance rockets, the

2

temperature of the hot gas is typically higher, resulting in higher heat transfer rates to the inner wall, and hence, higher steady state inner wall temperatures. With any significant increases in gas temperatures in today's rockets, the heat transfer to the coolant will be unable to keep up with the heat transferred from the hot gas, resulting in steady state inner wall temperatures in excess of the melting point of the nozzle wall material.

The goal of film and transpiration cooling is to reduce the amount of heat reaching the nozzle wall by cooling the boundary layer, enhancing its insulating properties. (see Fig 1.2)
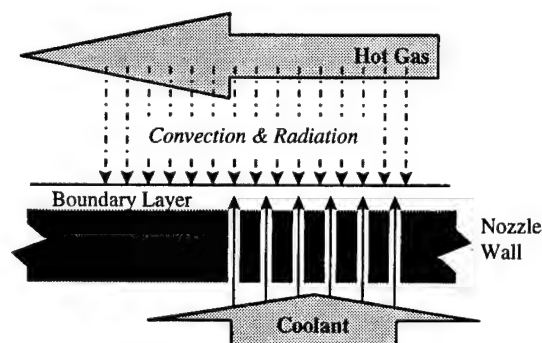
Figure 1.2 Schematic of Film and Transpiration Cooling

Heat transfer through the turbulent boundary layer of a supersonic nozzle is a very complex phenomena (Lenertz, 1994:2), as is the evaporation of a fluid on a surface with pressure and temperature gradients. Incropera and DeWitt (1996:331-2) address this problem:

> Our primary concern is still that of developing means to determine the convection coefficients h and h_m. Although these coefficients may be obtained by solving the boundary layer equations, it is only for simple flow situations that such solutions are readily effected. *The more practical approach frequently involves calculating h and h_m from empirical relations. The particular form of these equations is obtained by correlating measured convection heat and mass transfer results* in terms of appropriate dimensionless groups.

Analytical modeling of liquid transpiration cooling of a supersonic nozzle is very difficult with the current lack of experimental data. The aim of this research is to provide such data.

1.3 Summary of Current Knowledge

Transpiration cooling is not a new technology, but due to high implementation costs, research has been limited to a very basic level, and past experiments have been limited to simple applications. However, in recent years, the need for more powerful rockets stated in Section 1.1 has sparked many new studies of this type of cooling.

Transpiration cooling has been a subject of research since 1946, and the first full-scale demonstration of a transpiration-cooled combustion chamber was performed by Aerojet in 1967. Still, transpiration cooling has not been applied in practice to the combustion chamber or nozzle regions of large liquid rocket engines (Lenertz, 1994:3-5; Keener, 1994:5-10). This is primarily due to the steep pressure gradients along the inner wall of the nozzle. Coolant flowing through porous materials takes the path of least resistance, which is the path with the greatest pressure drop. Unfortunately, the areas with the *lowest* pressure drop (i.e., the areas along the inner wall of the nozzle with the highest pressures), such as the throat, tend to also be the hot spots. This creates the need for varying material porosity, thickness, or both to provide properly distributed cooling. The manufacture of such large, complex shapes of porous material is difficult and costly. Chen (1995) experimentally found reduced effects of this cooling distribution problem by reducing the axial distance (i.e., distance upstream or downstream of the throat) covered by the porous material. This problem can also be sidestepped to some degree with the application of platelets, rather than porous materials. Layers of platelets bonded or held together allow the creation of flow passages of any pattern, forcing more coolant to go where it is most needed. Although transpiration cooling has not yet been perfected enough to use along the nozzle wall, it has been used in some simpler applications, such as the injector faces of the J-2 (Saturn V upper stage) and Space Shuttle Main Engines.

Sreekanth and Reddy (1997) performed a numerical analysis of transpiration cooling using a two-dimensional, compressible Navier-Stokes code. Part of the study analyzed a flat plate for Mach numbers ranging from six to ten, and a range of blowing ratios. Coolant was assumed to be an ideal gas, and blowing ratio was defined as the ratio of mass injection rate to Stanton number. Results showed a 90% reduction in surface temperature could be achieved for the flat plate with blowing ratios above three. The authors surmised the reason for the limit was the initial temperature of the coolant. The study makes no reference to the impact these blowing ratios may have on the performance of a nozzle.

Landis (1995) performed a finite differencing model of both regenerative cooling and transpiration cooling and compared the results. He assumed a liquid coolant, but treated it as an ideal gas, thereby neglecting the effects of the endothermic evaporation process. Still, his model demonstrated a 35% reduction in wall temperatures for transpiration cooling over regenerative cooling, given an optimum combination of wall porosity, wall thermal conductivity, and blowing ratio. However, a potential problem identified was a very steep temperature gradient in the wall near the hot surface. This problem would possibly have been greatly reduced or eliminated had the model included the endothermic effects of evaporation, since the evaporation would take place near the hot surface where the temperature gradient problem was identified.

An Aerojet experimental comparison of liquid transpiration cooling and regenerative cooling was performed in 1991, using liquid RP-1 rocket fuel as the coolant (Lenertz, 1994:4). The study achieved a 97% reduction in heat flux at certain test conditions, while *increasing* the rocket's specific impulse. This performance improvement is primarily due to the elimination of the long, narrow channels used in regenerative cooling, which reduce the turbopump's available power to pressurize the chamber. This new found power can be applied to higher chamber pressures, increased turbopump lifetime, or a combination of both.

On-going research at the German Aerospace Research Establishment has provided a wide range of data on the transpiration cooling of an H_2/O_2 combustion chamber. So far, that research effort has used water and gaseous hydrogen as coolants over a range of chamber pressures from 0.5 to 1.5 MPa. The facility provides run times up to 15 seconds and variable coolant flow rates. In addition, the facility not only records wall surface temperature, but temperatures at various depths within the wall. Results of using water as a coolant showed the cooling to have a decreasing effect with increasing chamber pressure, with reductions in heat flux around 70% for 1.5 MPa chamber pressure. Another interesting result was 90% of the total heat transferred to the wall was absorbed by the coolant water in the first 2 mm of wall thickness. At a depth of 4 mm into the wall, zero heat flux was recorded. The research team plans to broaden its test matrix to include chamber pressures up to 10 MPa, other coolants, and various chamber geometries. (Lezuo and Haidn, 1996).

In the last few years, several other studies related to transpiration cooling have been performed that are not directly relevant to this research. For example, Choi et al (1997:1, 5) performed a transpiration cooling experiment using gaseous helium as coolant, forced through multiple layers of perforated metal sheets. Heat was radiated to the sheets via an arc-lamp. Temperature gradients associated with heat transfer rates above 230 $W/(cm^2$-s) caused the sheets to expand independently, choking off the coolant passageways. However, Raghuraman et al (1994:1-11) analyzed a form of platelet transpiration cooling that was successfully applied to the forebody of the High Endoatmospheric Defense Interceptor (HEDI). This method fused platelets together, and demonstrated surface temperature reductions over 50% under conditions where uncooled heat fluxes exceeded 2,300 $W/(cm^2$-s). Another study of the effects of transpiration cooling applied to the outside of a vehicle was performed by Ren et al (1997:1, 5). A computational analysis was performed on the boundary layer structure, but was limited to

6

laminar flow conditions. However, Kacynski & Hoffman (1994:1, 8-10) developed a computational model of a hydrogen/oxygen rocket engine with an H_2-transpiration-cooled plug-and-spool nozzle. The results agreed closely with experimental data acquired at NASA Lewis Research Center (LeRC) in the early 1970s, demonstrating this application of transpiration cooling to be very effective near the throat. It is important to note that the data acquired by LeRC was relatively incomplete, making it necessary to make several important simplifying assumptions in the computational model (Kacynski & Hoffman, 1994:9).

As described in this section, knowledge and understanding of transpiration cooling have been broadened by many new experiments and computational analyses in recent years. The results presented in Chapter 4 of this report build upon that knowledge base. The next section details this report's contribution to the field of transpiration cooling.

1.4 Scope and Objective

This research effort was intended to broaden the envelope of test conditions studied in the field of transpiration cooling. It does not involve blowing ratios as past research has, but rather surveys a wide range of test conditions, starting with higher stagnation properties than most previous studies.

Hazelton (1996) used a Mach 3.0 nozzle to generate flow for his test article. That same nozzle was modified to become the test article for this heat transfer experiment. Because of its multi-piece design, the diverging portion of the nozzle could be easily modified, but the converging portion could not. Therefore, the porous material and instrumentation began at the throat and continued to the nozzle exit. One surface thermocouple was positioned only 3.5 mm downstream of the throat with the hope to acquire good data as close to the throat as possible, but little cooling effect was seen here for two reasons: First, there was not enough porous material

7

upstream of the surface thermocouple to add significant mass to the boundary layer. Second, the porous material in this area was damaged to some degree in the process of fabricating the nozzle. Ultimately, no measurable cooling effect was seen at this surface thermocouple station, so this study was forced to focus on the effects seen further downstream of the throat.

Because of the short run times associated with the shock tunnel, concerns were raised regarding the liquid cooling system. Unlike previous transpiration cooling studies where air was used, forcing water through the wall prior to the shock would result in puddling. The effect of these puddles may not go away before the end of the steady state period. Also, there was a high potential for the puddles to run into the converging portion of the nozzle before the shock, creating more unknown effects. As a result of these concerns, it was hypothesized that simply saturating the wall before each run would provide enough water for the short run times involved. (Data later showed this to be a poor hypothesis. A dry-out effect was seen, shortening the period in which the cooling could be analyzed and raising questions of the applicability of this study to liquid transpiration cooling systems with forced coolant flow. This effect is discussed in more detail in Section 4.2.) With blowing ratio no longer a variable parameter as in previous transpiration cooling research, stagnation pressure and temperature were varied and a comparison made between the wetted nozzle and dry nozzle at each test condition. Stagnation pressure and temperature ranged from 2.0 to 5.2 MPa, and from 840 to 1315 K, respectively.

1.5 Methodology

The AFIT High Pressure Shock Tunnel was chosen for this experiment due to its capability of high pressures and very high temperatures not attainable in the other facilities available to AFIT students. The main drawback of the shock tunnel is the very short run times (on the order of 0.7 to 2.0 milliseconds). This drives the need for very fast instrumentation, so

the attached nozzle was outfitted with piezoresistive pressure transducers and fast-response coaxial surface-measuring thermocouples. Data were collected by a Nicolet 500 Data Acquisition System at a rate of one data point per microsecond. The porous side of the nozzle was the only side with instrumentation, so each test condition required runs with the nozzle wetted as well as runs with a dry nozzle to provide a control. With a dry nozzle, runs were very repeatable, so only three dry runs were performed at each test condition. However, when the nozzle was wetted, results tended to be less consistent, so more runs were necessary. Unfortunately, time constraints imposed a limit of five wet runs at each test condition.

For each individual run, the run time was determined from the stagnation pressure trace, measured at the nozzle entrance. A delay was noticed in the temperature traces as the incident shock traveled from one surface thermocouple to the next, so the shock arrival time at each surface thermocouple was determined from its own individual temperature trace. The time at which the effects of the shock itself had passed was also determined from this temperature trace. Data was processed by several computer programs to determine the heat transfer rate and then the convection heat transfer coefficient. The convection coefficient was then averaged over a steady state period. The data reduction process is outlined in more detail in section 3.6.

However, as with any experimental research, a fundamental understanding of the underlying theory must be reached before work begins to ensure the proper data is collected and a useful result is produced. The theory behind this experiment is presented in the next chapter.

II. Theory

2.1 Heat Transfer

The rate of convective heat transfer from combustion gasses to thrust chamber walls is difficult to calculate accurately because the boundary layer is strongly affected by wall curvature, axial pressure gradient, and the normal temperature gradients associated with high-intensity heat flux (Hill and Peterson, 1992:545). However, we are able to obtain a reasonable approximation by looking at the conduction aspect of the problem. By measuring the surface temperature history of the nozzle, the rate of heat flux conducted into the wall as a function of time can be determined from the equation

$$q''(t) = 2\left(\frac{\rho c k}{\pi}\right)^{1/2}\left[\sum_{j=1}^{J}\frac{T(t_j) - T(t_{j-1})}{(t_J - t_j)^{1/2} + (t_J - t_{j-1})^{1/2}}\right] \tag{2.1}$$

Lenertz (1994:51) provides a derivation of the integral form of Eq (2.1). Note Lenertz's derivation is for use with a heat flux gauge, which employs two mediums. However, once the derivation assumes the top medium is thin enough to neglect, it becomes applicable to the surface thermocouples used here.

Once the heat flux conducted into the wall is known, a portion of this heat is assumed to come from radiation. A simple radiation analysis was performed for each test condition using the Stefan-Boltzmann law

$$q_{rad}'' = \varepsilon\sigma(T_{aw}^4 - T_w^4) \tag{2.2}$$

where q_{rad}'' is the heat flux due to radiation from the hot gas to the nozzle wall, ε is emissivity, the measure of a surface's ability to emit and absorb radiation, and σ is the Stefan-Boltzmann constant ($\sigma = 5.67 \times 10^{-8}$ W/m^2 K^4). The adiabatic wall temperature, T_{aw}, is calculated as described in Section 2.4, and T_w is the nozzle wall surface temperature, averaged over the steady

10

state period. For each case, assuming $\varepsilon = 1$, heat flux due to radiation was found to be just under 7% of the total heat flux. Since $\varepsilon < 1$ for all real surfaces, the effect of radiation would actually be less than this.

The remaining heat transferred from the hot gas to the wall is due to convection, $q_{conv}'' = q'' - q_{rad}''$. The convection heat transfer coefficient as a function of time, $h(t)$, can then be found from a modified version of Newton's law of cooling,

$$q_{conv}'' (t) = h(t) (T_{aw} - T_w) \qquad (2.3)$$

However, because ε is not known for the porous material, this analysis assumes $q_{conv}'' = q''$, which introduces a fixed error in the values of $h(t)$ calculated using Eq (2.3). The calculated $h(t)$ values are known to be *up to* 7% high as a result of this assumption.

Once the time averaged convection heat transfer coefficient is known, it can be used in generating a theoretical temperature curve for comparison to the observed. Incropera and DeWitt (1996:237) provide a derivation of a relation to generate such a curve, starting with the 1-D heat equation for a plane wall with no heat generation (the conduction is assumed to be 1-D given the short run times and similar thermal conductivities of the chromel thermocouple tube and porous stainless steel),

$$\frac{\partial^2 T}{\partial x^2} = \frac{1}{\alpha} \frac{\partial T}{\partial t} \qquad (2.4)$$

Introducing the similarity variable, $\eta = x / (4\alpha t)^{1/2}$, and substituting into Eq (2.4), the heat equation becomes

$$\frac{\partial^2 T}{\partial \eta^2} = -2\eta \frac{\partial T}{\partial \eta} \qquad (2.5)$$

The wall is assumed to be a semi-infinite solid with both the initial condition and interior boundary condition expressed as

$$T(\eta \to \infty) = T_i \tag{2.6}$$

With exposure to sudden surface convection, the surface boundary condition is

$$-k\left(\frac{\partial T}{\partial \eta}\right)_{\eta=0} = h\left[T_{aw} - T(0)\right] \tag{2.7}$$

Solving the system results in the equation

$$\frac{T(x,t) - T_i}{T_{aw} - T_i} = \operatorname{erfc}\left(\frac{x}{2\sqrt{\alpha t}}\right) - \left[\exp\left(\frac{hx}{k} + \frac{h^2\alpha t}{k^2}\right)\right]\left[\operatorname{erfc}\left(\frac{x}{2\sqrt{\alpha t}} + \frac{h\sqrt{\alpha t}}{k}\right)\right] \tag{2.8}$$

Since we are concerned only with the surface temperature, we set $x = 0$, and Eq (2.8) simplifies to

$$T(0,t) = (T_{aw} - T_i)\left\{1 - \left[\exp\left(\frac{h^2\alpha t}{k^2}\right)\right]\left[\operatorname{erfc}\left(\frac{h\sqrt{\alpha t}}{k}\right)\right]\right\} + T_i \tag{2.9}$$

2.2 Liquid Transpiration Cooling

Incropera and DeWitt (1996:325) provide a very clear description of the physical phenomena taking place during liquid transpiration cooling, referred to here as *evaporative* cooling:

> Evaporative cooling occurs whenever a gas flows over a liquid. Evaporation must occur from the liquid surface, and the energy associated with the phase change is the latent heat of vaporization of the liquid. Evaporation occurs when liquid molecules near the surface experience collisions that increase their energy above that needed to overcome the surface binding energy. The energy required to sustain the evaporation must come from the internal energy of the liquid, which then must experience a reduction in temperature (the cooling effect). However, if steady-state conditions are to be maintained, the latent energy lost by the liquid because of evaporation must be replenished by energy transfer to the liquid from its surroundings.

This energy transfer from the surroundings to the liquid, coupled with the cooled fluid entering the boundary layer, produces the desired nozzle wall cooling effect. Applying conservation of energy to the control volume in Fig 2.1,
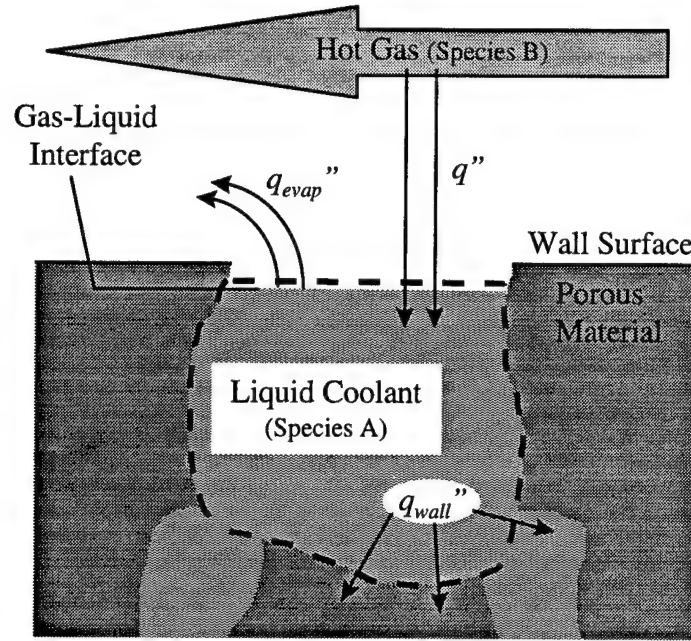
Figure 2.1 Control Volume About the Coolant in a Single Pore

$$q'' = q_{evap}'' + q_{wall}'' \qquad (2.10)$$

Eq (2.10) simply states all the energy transfer from the hot gas (per unit area) that is not absorbed

by evaporation must be transferred to the nozzle wall material (or to coolant deeper inside the

wall). The energy absorbed by evaporation can be approximated as

$$q_{evap}'' = n_A'' h_{fg} \qquad (2.11)$$

where h_{fg} is the latent heat of vaporization of the liquid, and n_A'' is the coolant mass flux from the

liquid to the gas, which can be determined from

$$n_A'' = h_m(\rho_{A,w} - \rho_{A,\infty}) \qquad (2.12)$$

where h_m is the convection mass transfer coefficient, and ρ_A is the density of the coolant at the

wall surface or in the freestream. Density of the coolant at the surface may be determined from

thermodynamic tables as a function of surface temperature (Incropera and DeWitt, 1996:286).

Surface temperature is nearly constant throughout testing, so the same is implied of coolant

density at the surface. h_m is proportional to the binary diffusion coefficient and the coolant density gradient normal to the surface,

$$h_m \propto -D_{AB}\left(\frac{\partial \rho_A}{\partial y}\right)_{y=0}$$

(2.13)

Assuming ideal gas behavior, kinetic theory has shown

$$D_{AB} \propto P^{-1}T^{3/2}$$

(2.14)

Surface temperature is appropriate to use in Eq (2.14), which experienced only small changes during shock tunnel runs. So taking T as constant, D_{AB} is shown to *decrease* with increasing pressures. The density gradient in Eq (2.13) can be determined from the concentration boundary layer equations, which show this gradient to be most strongly dependent on the velocity field. (Incropera and DeWitt, 1996:292, 310, 791) Since the nozzle dimensions do not change and the flow is choked, the velocity field does not change with pressure, and changes in the coolant density gradient are taken to be very small with changes in pressure. This leads to the conclusion that, for the conditions of this experiment, *h_m and n_A'' are inversely proportional to pressure.*

The mass flux could also be easily determined experimentally if the test facility provides long enough run times to accommodate a positive coolant feed. In such a case, the mass flux could be found from measurements of the amount of coolant forced through the system.

2.3 Shock Tunnel Relations

The shock tunnel is used here to generate high-pressure, high-temperature stagnation conditions at the entrance of the nozzle. The stagnation conditions can be predicted using the following relations:

14

$$\frac{P_5}{P_1} = \left[\frac{2\gamma M^2 - (\gamma - 1)}{\gamma + 1}\right]\left[\frac{(3\gamma - 1)M^2 - 2(\gamma - 1)}{(\gamma - 1)M^2 + 2}\right]$$

(2.15)

$$\frac{T_5}{T_1} = \frac{\left[2(\gamma - 1)M^2 + (3 - \gamma)\right]\left[(3\gamma - 1)M^2 - 2(\gamma - 1)\right]}{(\gamma + 1)^2 M^2}$$

(2.16)

where M is the Mach number of the incident shock wave, γ is the ratio of specific heats of the driven gas (assumed to be 1.4 for air), and the subscripts 1 and 5 represent the initial driven gas conditions and the conditions at the nozzle entrance after shock reflection, respectively (Vlcek, 1994:9). The Mach number of the incident shock is calculated by measuring its velocity with two pressure transducers positioned a known distance apart in the tunnel and calculating the speed of sound based on the initial temperature of the driven gas.

The actual stagnation pressure, P_o, and temperature, T_o, are typically less than the values of P_5 and T_5 predicted by Eqs (2.15) and (2.16) due to part of the shock being "swallowed" by the nozzle, losses in the diaphragm rupturing process, boundary layer growth, shock attenuation, and other real gas effects (Vlcek, 1994:9). To account for these losses, P_o is measured by a pressure transducer at the entrance of the nozzle. Losses in temperature are then approximated as proportional to the losses in pressure (Vlcek, 1995:31), so T_o is calculated from

$$\frac{T_o}{T_5} = \frac{P_o}{P_5}$$

(2.17)

Once P_o and T_o are known, conditions throughout the nozzle can be determined.

2.4 Nozzle Fluid Flow Relations

Knowledge of the stagnation conditions and the nozzle dimensions allows the determination of the flow conditions everywhere in the nozzle. So at each thermocouple

position, the gas temperature could be determined from the local Mach number, which is given by the isentropic relation

$$\frac{A}{A_t} = \frac{1}{M}\left[\frac{2}{\gamma+1}\left(1+\frac{\gamma-1}{2}M^2\right)\right]^{\frac{\gamma+1}{2(\gamma-1)}}$$

(2.18)

Now with T_o and M known, The local freestream static temperature, T_g, can be found from (Hill and Peterson, 1992:70-71)

$$\frac{T_o}{T_g} = 1 + \frac{\gamma-1}{2}M^2$$

(2.19)

For high-speed nozzle flows, viscous effects cause an increase in gas temperature near the wall. Therefore, when considering the heat transfer to the wall, one must use the *adiabatic wall temperature*, T_{aw}, in lieu of T_g. T_{aw} is related to T_g and T_o by a recovery factor, r, which is defined by

$$r = \frac{T_{aw} - T_g}{T_o - T_g} = Pr^{1/3}$$

(2.20)

For compressible turbulent boundary layers up to Mach numbers of 4, the recovery factor is about 0.91 for typical rocket propellants. (Hill and Peterson, 1992:546)

Eqs (2.19) and (2.20) may be combined to form a direct calculation of T_{aw}

$$T_{aw} = T_g\left[1 + \frac{r(\gamma-1)}{2}M^2\right]$$

(2.21)

This adiabatic wall temperature is then used in the determination of the convection heat transfer coefficient as described in Section 2.1.

A simple analysis was performed on the nozzle to ensure it would be "started" for all the conditions tested. It was found the nozzle would be supersonic for stagnation pressures above

16

0.19 MPa and a shock would not be present inside the nozzle at stagnation pressures above 0.36 MPa. These conditions are well below those tested in this experiment.

The various theoretical relations above make way for a better understanding of how the facility described in the next chapter can be used to obtain and process temperature data to generate the desired heat transfer information.

III. Experimental Apparatus and Procedure

This experiment was performed using the AFIT High Pressure Shock Tunnel with Helium as the driver gas. The test section was a nozzle attached to the end of the shock tunnel, and pressure and temperature data was collected by a Nicolet 500 Data Acquisition System. This chapter details the components of this setup and how they were used.

3.1 Mach 3 Nozzle

The test section in this experiment was the diverging portion of a Mach 3.0 nozzle (see Fig 3.1(a)). From the nozzle throat to the exit, it is two-dimensional with a flat lower surface, a contoured upper surface, and flat, plexiglass sides. The lower surface is fitted with a 0.060 inch-thick piece of porous stainless steel to be saturated with liquid coolant.
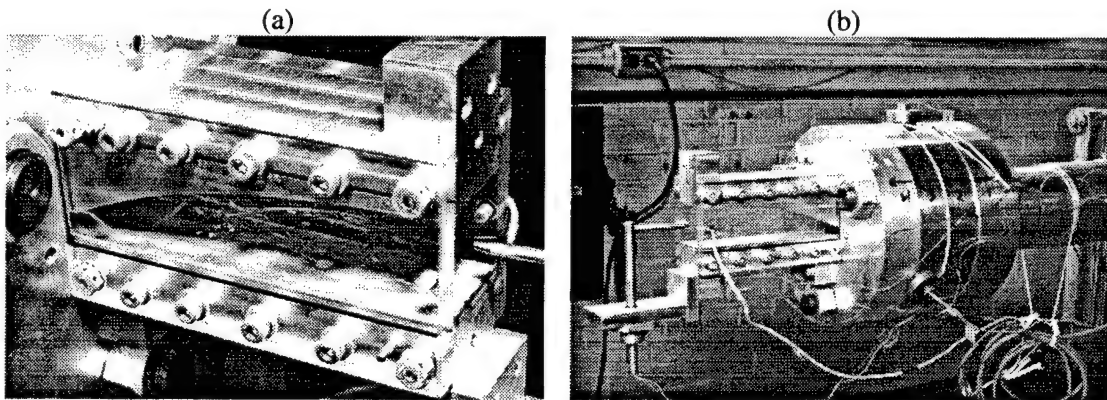
Figure 3.1 (a) Diverging Nozzle Test Section. (b) Nozzle, Including Transitionary Flanges and the End of the Shock Tunnel.

The view in Fig 3.1 (b) shows the end of the two-inch inner diameter shock tunnel and the flanges which house instrumentation. The last flange (marked "4") is contoured to make the converging portion of the nozzle and the transition from axisymetric to two-dimensional. The

point where this flange mates with the two-dimensional piece is the throat of the nozzle. This point is identified in Fig 3.2 as "x = 0." The height of the throat is 0.356". Fig 3.2 also shows the positions of the instrumentation. With x oriented as shown in Fig 3.2, surface thermocouple stations 1, 2, 3, and 4 are located at x = 0.14 in, 1.95 in, 3.76 in, and 5.57 in, respectively.
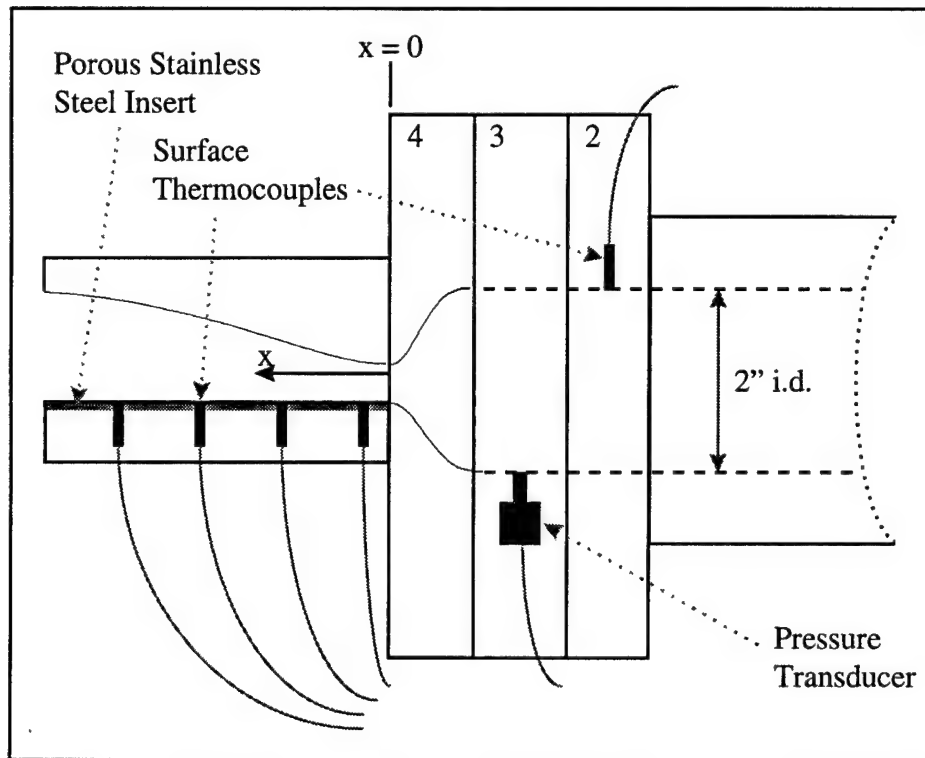
Figure 3.2 Nozzle Schematic (not to scale).

The porous stainless steel insert in the nozzle was wetted using a simple, 3-step procedure. First, a sponge cut to the size of the porous insert was soaked in distilled water and lain flat on the porous metal. The sponge was then supersaturated by squirting additional distilled water onto it. The sponge was left in place for several minutes. Second, the sponge was removed quickly, leaving puddles on the porous metal. The metal was given several more minutes to soak up as much water from the puddles as possible. Third, the wet sponge was put back in place and slid out carefully, at a rate just right to leave tiny beads of water behind on the

surface of the porous metal. Carefully following this procedure and then waiting one minute resulted in most (but not all) of these tiny beads of water being absorbed into the porous metal.

3.2 Coaxial Thermocouples

Surface temperatures were measured in this experiment by Medtherm fast-response type-E coaxial thermocouples. These thermocouples consist of a cylindrical chromel tube, a constantan center wire, and a thin layer of insulation between the two metals. Once prepared for operation, the end of the tube served as the sensing surface. To prepare each thermocouple, 300-grit sand paper was dragged across the end of the tube in a uniform direction. This was repeated until the measured resistance from one thermocouple lead to the other was very small. This process drags slivers of metal across the layer of insulation, "cold welding" a junction from the tube to the center wire. These slivers are as thin as one micron, allowing the thermocouples' response to temperature changes to be as fast as one microsecond.
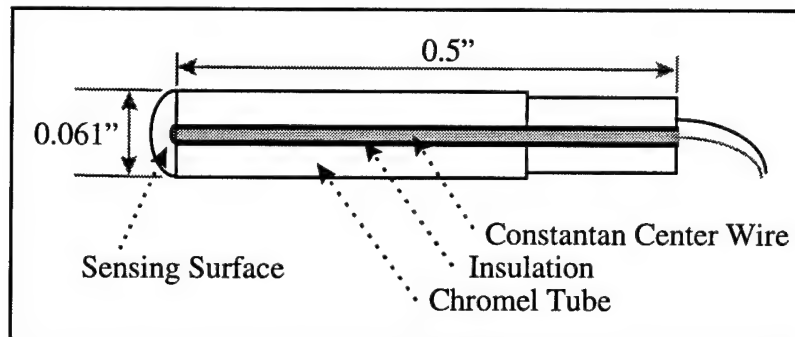
Figure 3.3 Coaxial Thermocouple – Cutaway View (not to scale)

The tube of a coaxial thermocouple comprises most of the mass of the instrument. Therefore, the thermophysical properties of the tube were used in determining the heat transferred to the thermocouple (and hence, to the nozzle wall). The tube of a type-E coaxial thermocouple is made of chromel, an alloy of nickel and chromium. Thermophysical properties

20

of this alloy in the temperature range tested, as calculated by the manufacturer, are (Medtherm, 1997)

Density: $\rho = 8730 \ \text{kg/m}^3$

Specific Heat: $c = 426.4 \ \text{J/kg K}$

Thermal Conductivity: $k = 17.3 \ \text{W/m K}$

3.3 Shock Tunnel

The AFIT High Pressure Shock Tunnel was used to generate the stagnation conditions for the Mach three nozzle. For this experiment, the tunnel was configured with a 10-foot-long driver section and a 20-foot-long driven section. A photograph of the entire facility is in Fig 3.4. A closer view of the driver is in Fig 3.5, shown disconnected from the driven, with the double diaphragm assembly in place. The high pressure control valves and plumbing for the shock tunnel are mounted to the base of the tripods supporting the driver. A detailed schematic diagram of this plumbing is in Fig 3.6. Shop air at 100 psig is supplied to the pneumatic valves by the bundle of hoses seen entering Fig 3.5 from the bottom. This bundle of hoses runs to a shop air manifold that is controlled electrically from the control panel in Fig 3.7. High pressure helium is supplied to the system by the high pressure hose seen entering Fig 3.5 from the right. This hose runs to the helium bottle farm in Fig 3.8.

The double diaphragm assembly is the firing mechanism for this shock tunnel. The region between the two mylar diaphragms is pressurized to over half the rupture pressure of each diaphragm, and the driver section is then pressurized to the desired pressure, which must exceed the diaphragm rupture pressure. The region between the two diaphragms is then vented to the outside atmosphere, causing the driver side diaphragm to rupture. The resulting shock wave then ruptures the driven side diaphragm, and the shock wave travels down the driven section. The

21

double diaphragm assembly (Fig 3.9 (a)) is a removable part of the driver. It is disassembled, as seen in Fig 3.9 (b), to replace the ruptured diaphragms.
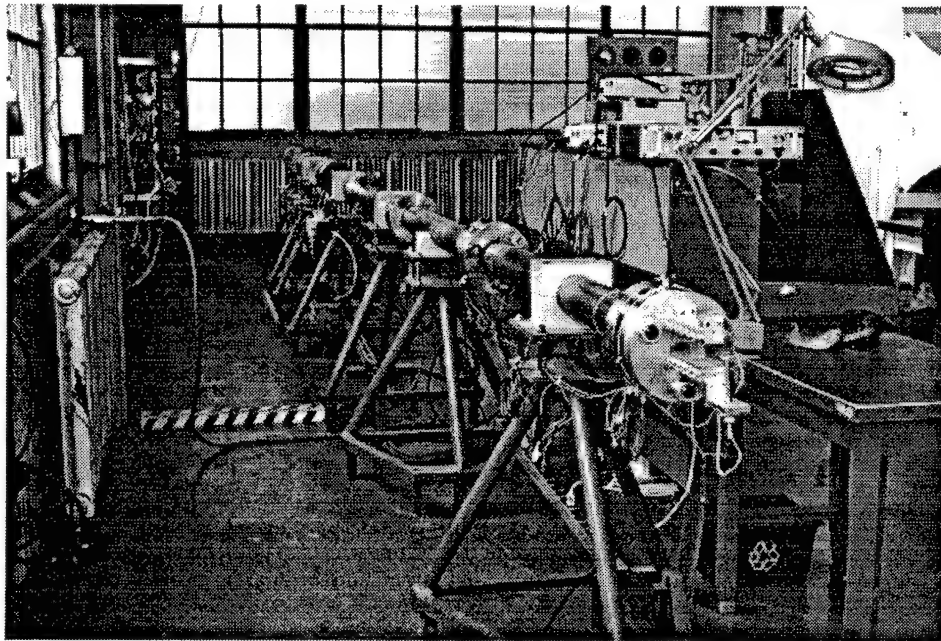
Figure 3.4 AFIT High Pressure Shock Tunnel
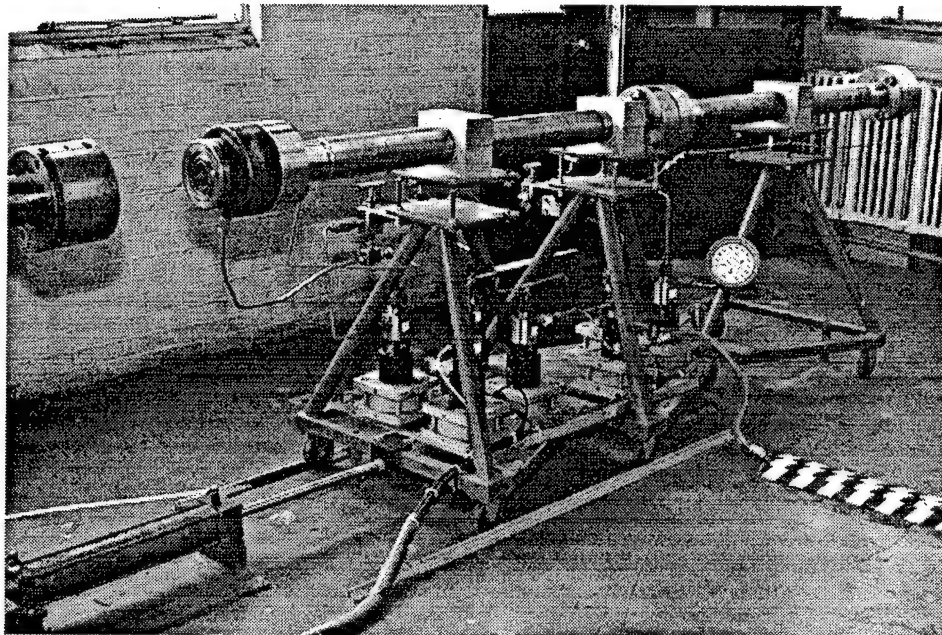
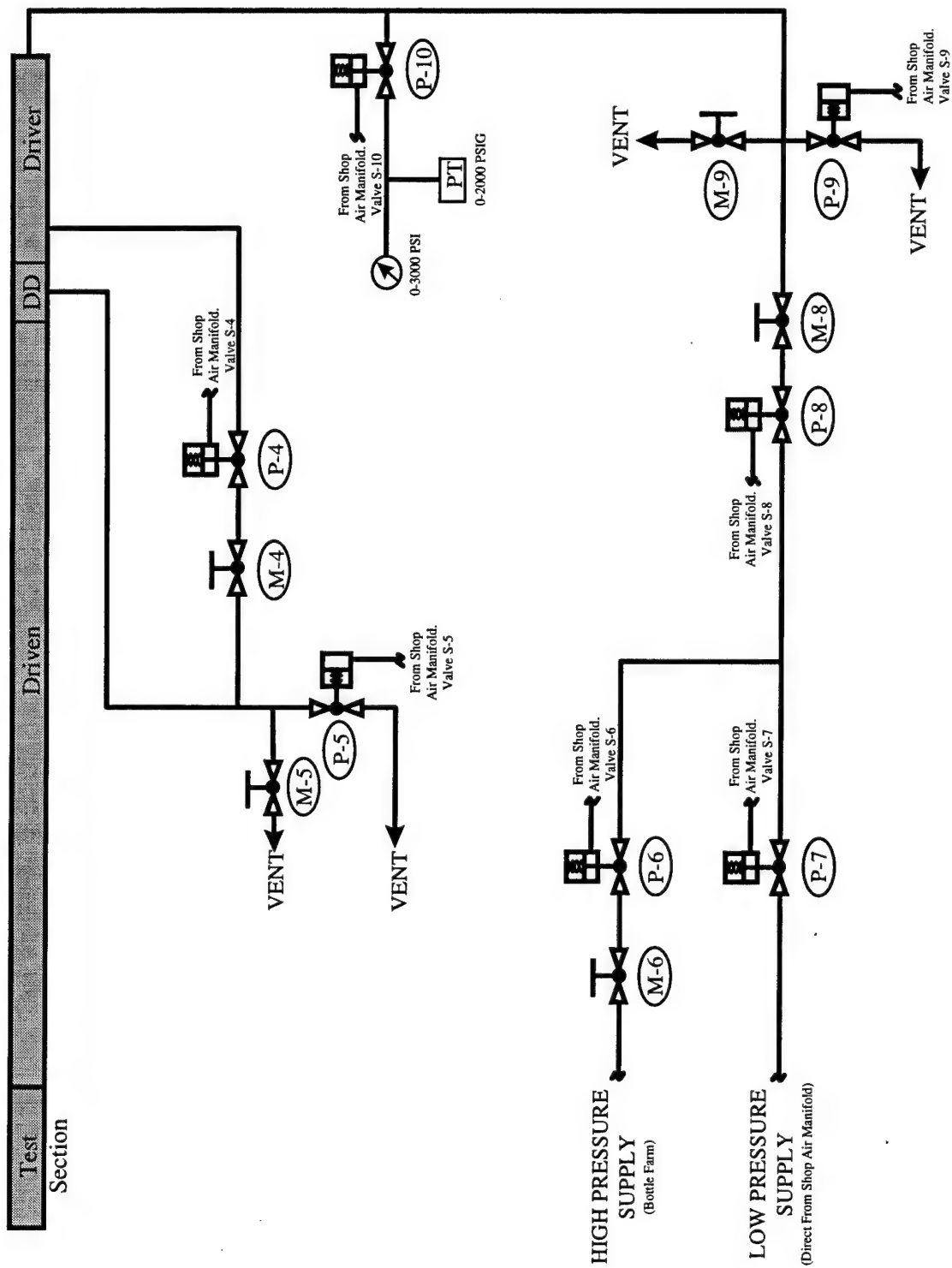**Figure 3.5** Driver Section and Pneumatic Control Valves

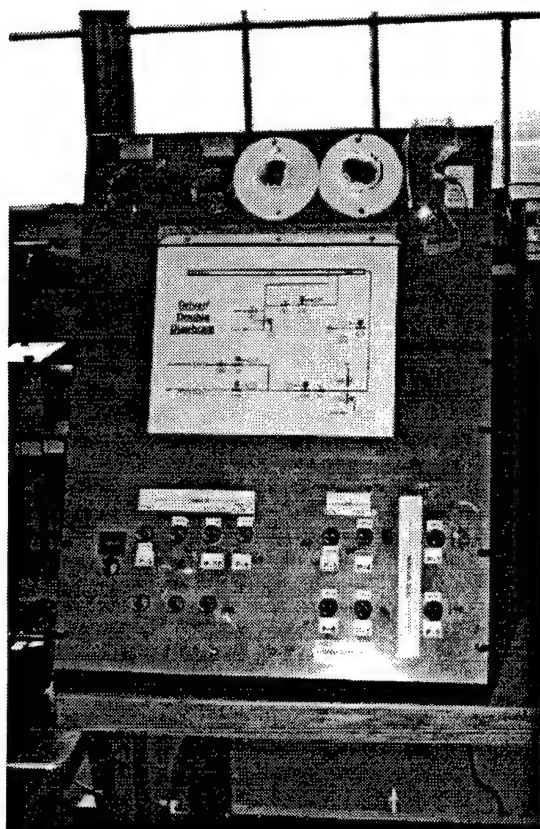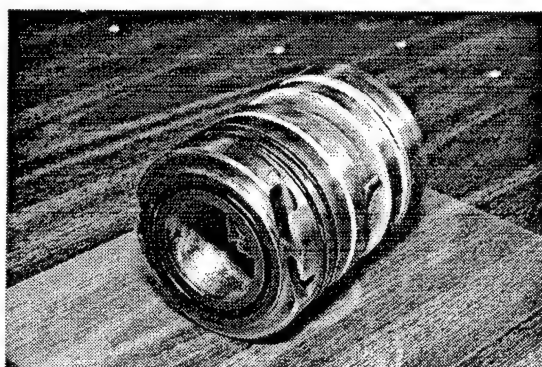**Figure 3.6** AFIT High Pressure Shock Tunnel Control Valve Schematic

Figure 3.7 Valve Control Panel
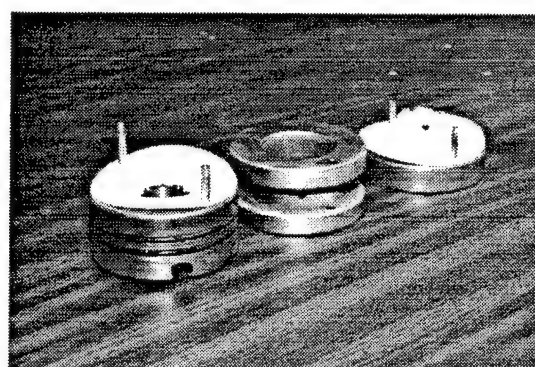

Figure 3.8 Helium Bottle Farm

(a)

(b)

Figure 3.9 Double Diaphragm Section, (a) assembled, and
(b) disassembled, ready for diaphragm replacement

3.4 Calibration

Very little calibration was necessary for the instrumentation used in this experiment. The coaxial thermocouples used a standard polynomial curve fit for type E thermocouples. The voltage-to-temperature relation is given by (Omega, 1993:A7)

$$T = C_0 + C_1E + C_2E^2 + C_3E^3 + C_4E^4 + C_5E^5 + C_6E^6 + C_7E^7 + C_8E^8 + C_9E^9$$

where E is microvolts, T is temperature in Kelvin, and the constants are

$C_0 =$ 273.15
$C_1 =$ 1.7057035×10^{-2}
$C_2 = -2.3301759 \times 10^{-7}$
$C_3 =$ $6.5435585 \times 10^{-12}$
$C_4 = -7.3562749 \times 10^{-17}$
$C_5 = -1.7896001 \times 10^{-21}$
$C_6 =$ $8.4036165 \times 10^{-26}$
$C_7 = -1.3735879 \times 10^{-30}$
$C_8 =$ $1.0629823 \times 10^{-35}$
$C_9 = -3.2447087 \times 10^{-41}$

To confirm proper operation of the thermocouples each day, before the shock tunnel was fired, the measured output of each thermocouple was compared to the room temperature given by a standard mercury thermometer. Each time, all thermocouples were within 1 K of each other and the thermometer. The small differences between each thermocouple's output are insignificant because the heat transfer at each thermocouple station was calculated based on the initial temperature measured by that station's thermocouple.

Three pressure transducers were used with the shock tunnel. The first measured driver pressure, and was roughly calibrated with an analog pressure gauge. This transducer and gauge are identified in Fig 3.6 at valve P-10. The calibration constant used was 0.635 mV/psig. Driver pressure was not used in any of the calculations supporting this experiment, so this rough calibration was used only to ensure consistency between runs.

The second pressure transducer, Endevco model number 8510B-500, measured driven pressure approximately five feet upstream of the nozzle entrance. While the pressure data from

this transducer was not used, the sudden jump in pressure indicated the time at which the incident shock wave passed its position. For this reason, this gauge was not calibrated at all.

The third pressure transducer measured the pressure of the stagnant air at the nozzle entrance. This is the pressure transducer shown in Fig 3.2. This transducer was an Endevco model number 8510B-2000, married to an Endevco signal conditioner, model number 4428A. This transducer and signal conditioner set was designed by Endevco to work together and eliminate the need for calibration by the customer. However, a few points below 100 psig were checked, confirming proper operation of the system. The system was set to provide 0.146 mV/psig.

3.5 Data Collection

Data was collected by a Nicolet 500 Data Acquisition System. Figure 3.10 shows the wiring schematic for data collection. Thermocouple wires and pressure transducer wires are marked with a T and a P, respectively. Voltages for the temperature and pressure traces were automatically displayed on the computer monitor. For each run, each channel generated a file specifically for use with the Nicolet software.

Each run required the following procedure. For each wet run, the porous nozzle wall was wetted via the method described in Section 3.1. The appropriate number of diaphragms were cut and installed in the double diaphragm (DD) assembly. The assembly was placed in the driver and the driver was moved by a pneumatic actuator to meet the driven. A large collar was tightened, sealing the two sections together. Then the Helium supply pressure was adjusted as appropriate, and the Nicolet system armed. The vent valves (P-5 and P-9) were closed, transducer valve (P-10) opened, DD isolation valve (P-4) opened, and high pressure supply valve (P-6) opened. The pressure was then controlled by opening the supply valve (P-8) until the
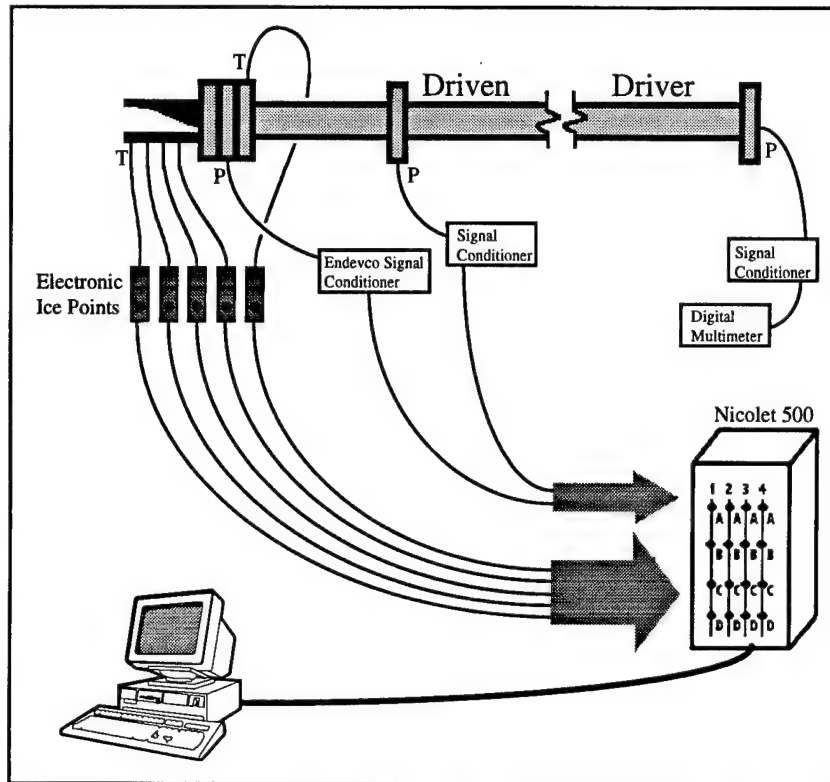
Figure 3.10 Data Collection Schematic

digital multimeter read a predetermined desired voltage. Once the pressure exceeded half the

desired driver pressure, the supply valve was closed, and then the DD isolation valve closed.

The supply valve was reopened until the desired driver pressure was reached. To fire the shock

tube, the DD vent valve (P-5) was opened. When no problems were encountered, this process

took about 20 to 25 minutes.

3.6 Data Reduction

The data files generated by the Nicolet system were processed by several computer

programs. First, a Nicolet program called *wft2flt.exe* was run to convert the file into one readable

by common software. The resulting file was a two-column data file, the first column being

voltage, and the second column time. This file was then imported into Microsoft Excel, where

the name was changed to a standard format which could be read by the data reduction programs, the time column was deleted, and the file saved as a text file. The time column could be deleted because the data reduction programs made use of the fact that the Nicolet 500 was always set to capture data at the rate of one point per microsecond.

A Matlab program called *reduce.m* (see Appendix B) was then run, which read in the text file, converted the voltage to temperature in Kelvin, filtered the temperature data, cropped the data set before and after the period of interest, and saved this new filtered and reduced data set to a new text file. The filter reduced high frequency noise by simply averaging each data point with the 25 preceding and 25 succeeding points. Trial and error showed this to be the smallest number of points that could be averaged to significantly reduce the noise.

Another Matlab program called *viewtemp.m* (see Appendix B) then plotted the temperature history resulting from *reduce.m*, allowing the user to zoom in and identify specific times of interest. These included the time at which the effects of the shock had passed, and for wet runs, the time at which the slope of the temperature history changed (as discussed in Section 4.2).

At this point, all the necessary information had been obtained to run a Matlab program called *convec.m* (see Appendix B). This is the program that input the temperature history resulting from *reduce.m* and calculated all the heat transfer data used to analyze the effects of liquid transpiration cooling.

The algorithm used by *convec.m* to calculate the convection heat transfer coefficient, h, was tested by another Matlab program, *tester.m* (see Appendix B). This program generated a theoretical temperature history, using Eq (2.9), based on a selected value of h. The program then used the *convec.m* algorithm to "back out" h from this theoretical temperature history. Within

six time increments, *tester.m* returned the same value of h used to generate the temperature history, thereby validating the algorithm used.

The procedure described above was necessary for each individual thermocouple's temperature trace for each run. Resulting heat transfer data and analysis for thermocouple stations two and three are presented in the next chapter.

IV. Results and Discussion

This chapter presents some typical temperature data collected and the calculated convection heat transfer coefficients for all conditions tested. Data collected at thermocouple station one (nearest the throat) are not presented for reasons discussed in Section 1.4. Results presented are for data collected at stations two and three, and comparisons are made between dry and wet cases.

4.1 Uncooled Heat Flux

Representing typical results for dry nozzle runs, the temperature and calculated heat flux histories for run 77 are shown in Fig 4.1. Brackets in the plots represent the beginning and end of the steady state period. The beginning of this period is determined from the temperature trace itself, and the duration is determined from the stagnation pressure trace, measured at the nozzle entrance. Stagnation conditions for this run were $P_o = 5.1$ MPa and $T_o = 1300$ K. The actual temperature history in Figure 4.1(a) has been filtered as described in Sec 3.6. Fig 4.1(b) shows $h_u(t)$ as calculated from the actual temperature history using Eqs (2.1) and (2.3). The subscript u indicates uncooled conditions. The average h_u over the steady state period was calculated as 2000 W/m^2 K, and used in Eq (2.9) to generate the theoretical temperature history in Fig 4.1(a). Note the excellent agreement between actual and theoretical temperature histories, attributed to good knowledge of ρ, c, and k for the thermocouple substrate. The qualitative attributes of Fig 4.1(a) also agree closely with that of Figure 4 of Lezuo and Haidn (1996:8). However, the calculated values of h_u were low compared to those predicted by Bartz's equation by a factor of two to three.

30
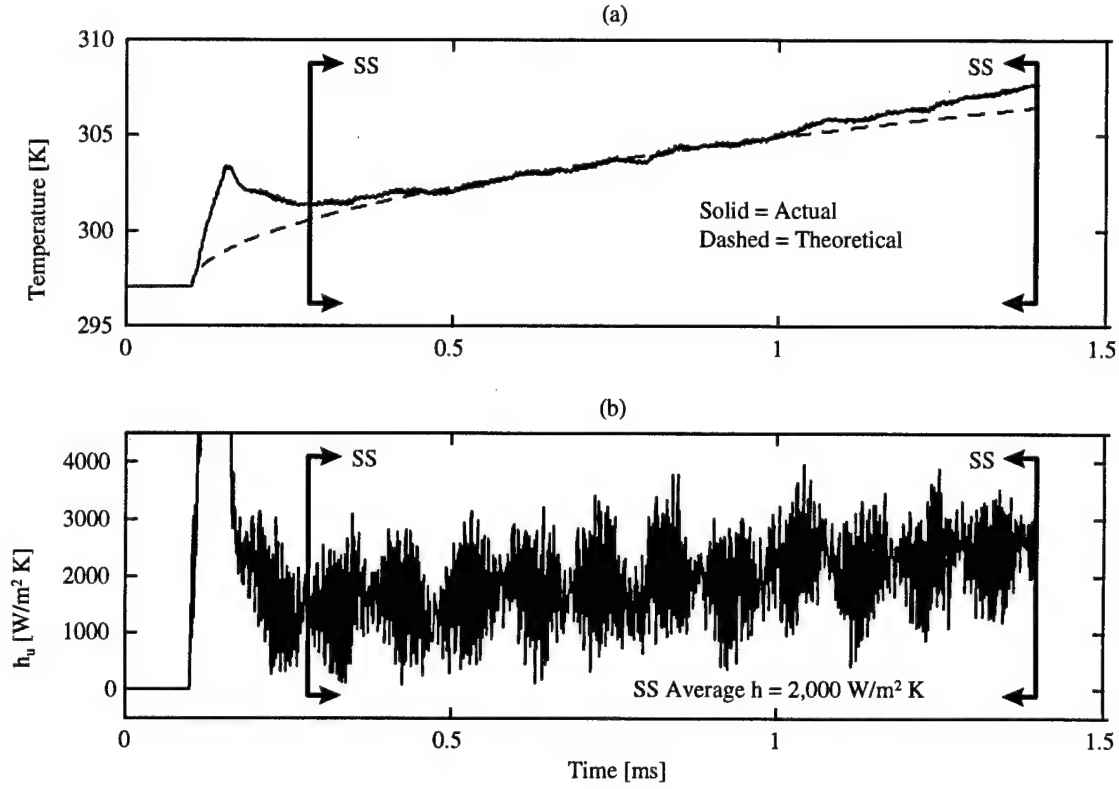
Figure 4.1 Representative Dry Run Results. Run 77, Thermocouple Station 2
$P_o = 5.1$ MPa, $T_o = 1300$ K

The discrepancy is likely due to several approximations made in applying Bartz's equation,

$$h = 0.026 \left(\frac{\mu^{0.2} c_p}{Pr^{0.6}} \right)_o \left(\frac{P_o}{c_{star}} \right)^{0.8} (D_t r_c)^{-0.1} \left(\frac{A_t}{A} \right)^{0.9} \varpi$$

(4.1)

where c_{star} is the characteristic velocity, D_t is the throat diameter, r_c is the throat radius of curvature, and

$$\varpi = \left\{ \left[\frac{T_w}{2T_o} \left(1 + \frac{\gamma - 1}{2} M^2 \right) + \frac{1}{2} \right]^{0.8 - 0.2a} \left(1 + \frac{\gamma - 1}{2} M^2 \right)^{0.2a} \right\}^{-1}$$

(4.2)

where a is the exponent of the viscosity-temperature relation $\mu \alpha T^a$ (a = 0.6 for diatomic gasses). (Hill and Peterson, 1992:550) Not all of the primary flow properties were well determined in

31

this study, thus approximations were required for μ, c_p, and Pr. In addition, the r_c in Eq (4.1) is intended to be the throat radius of curvature of an axisymetric nozzle. Therefore, r_c for the 2-D nozzle used here (see Figs 3.1(a) and 3.2) requires a conversion factor to account for this geometry difference and be properly applied in Eq (4.1). Hill and Peterson (1992:551) also note that, due to test results that contradict predictions by Eq (4.1), "the complete validity of equations of this type is not certain." So the values of h calculated here were chosen in favor of calibrating them to agree with Bartz's predictions due to the excellent agreement in Fig 4.1(a), and the facts that ρ, c, and k are well known, and there were very few additional assumptions or approximations made in the method described in Chapter 2.

The convection coefficients at Stations two and three for all dry runs are plotted in Fig 4.2. Results increased approximately linearly with increasing stagnation pressure. This is an expected result because the increase in pressure is accompanied by an increase in temperature as well as an increase in density. This density increase causes an increase in Reynolds number ($Re_L = \rho VL/\mu$) throughout the flow. In turbulent flow, Nusselt number ($Nu_L = hL/k_f$) is known to vary with Reynolds number according to (Incropera and DeWitt,1996:355)

$$Nu_L = 0.0296 \, Re_L^{4/5} \, Pr^{1/3} \tag{4.3}$$

The lines represent the average values for each stagnation condition, also given in Table 4.1.

Table 4.1 Convection Coefficient (Dry Nozzle)

P_o [MPa]	Station 2		Station 3	
	h [W/m² K]	Std Dev	h [W/m² K]	Std Dev
1.99	840	40	890	40
2.54	1210	160	1250	20
3.00	1220	40	1330	50
3.53	1470	40	1650	50
3.85	1490	60	1710	20
4.51	1800	40	2080	30
4.76	1830	140	2110	100
5.16	1950	50	2270	110
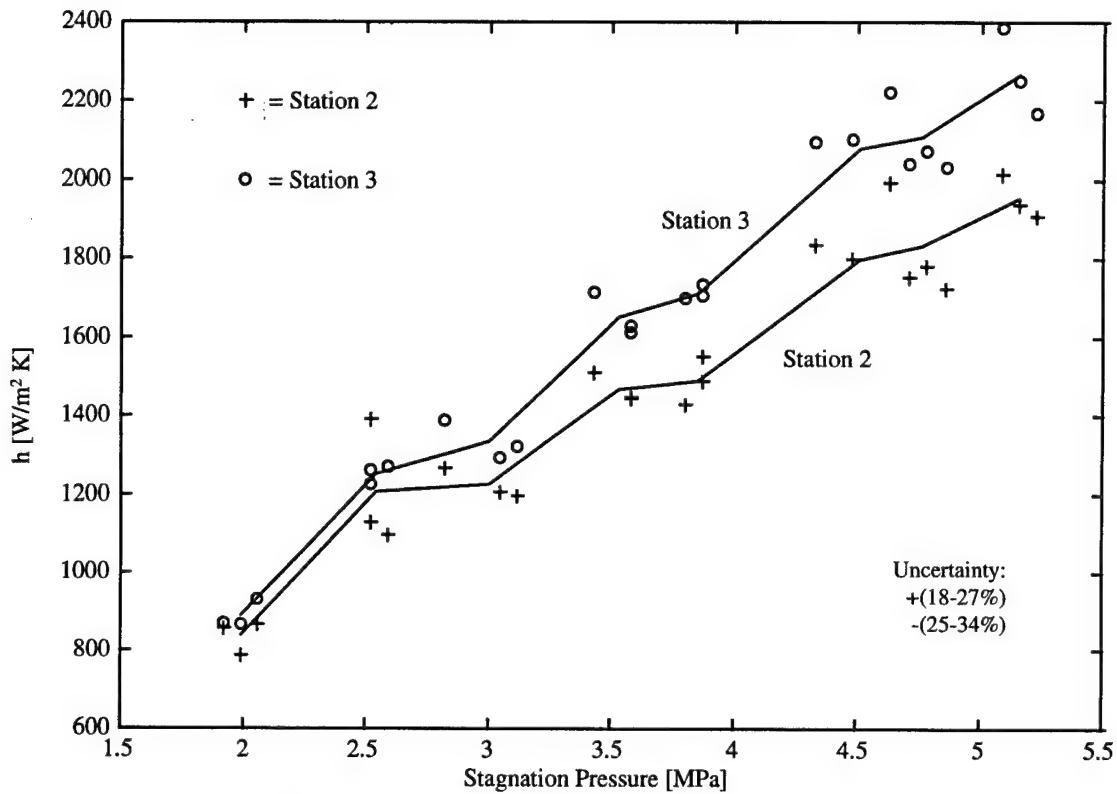
Figure 4.2 Convection Coefficient (Dry Nozzle)

Since peak heat flux is expected at the throat (Hill and Peterson, 1992:550), it is also expected that heat flux should decrease with distance from the throat. However, the plots in Fig 4.2 contradict this expectation. One possible explanation of this result may be the transition from a laminar boundary layer to a turbulent boundary layer. While the cause of this result is worthy of investigation, time constraints prevented its investigation in this report.

4.2 Effect of Liquid Transpiration Cooling

An example of the temperature history and calculated convection coefficient history for a wetted nozzle run is displayed in Fig 4.3. The plots shown are for run 28, which was among the lower-pressure runs where the effect of the liquid transpiration cooling was strongest. In Fig 4.3(a), note the two distinct slopes of the temperature curve after the shock passes. The first

bracket on the temperature curve indicates the start of the steady state period. The surface temperature for this run decreases as the water cools the surface. The second bracket represents the point at which the water has evaporated to a critical depth within the porous wall. Below this depth, the primary flow is unable to "wick" the water up fast enough to sustain the cooling effect. After this point, the temperature increases as if the cooling were negligible. (This is the dry-out effect referred to in Section 1.4.) The third bracket represents the end of the steady state period.

This temperature trace was used to calculate the convection coefficient, h(t), using Eqs (2.1) and (2.3). Resulting values are plotted in Fig 4.3(b). h(t) was then averaged over the two regions (i.e., *region 1* from the first to second bracket, and *region 2* from the second to third bracket). These averages are denoted $h_{c,1}$ and $h_{c,2}$ respectively, and are shown in Fig 4.3(b).
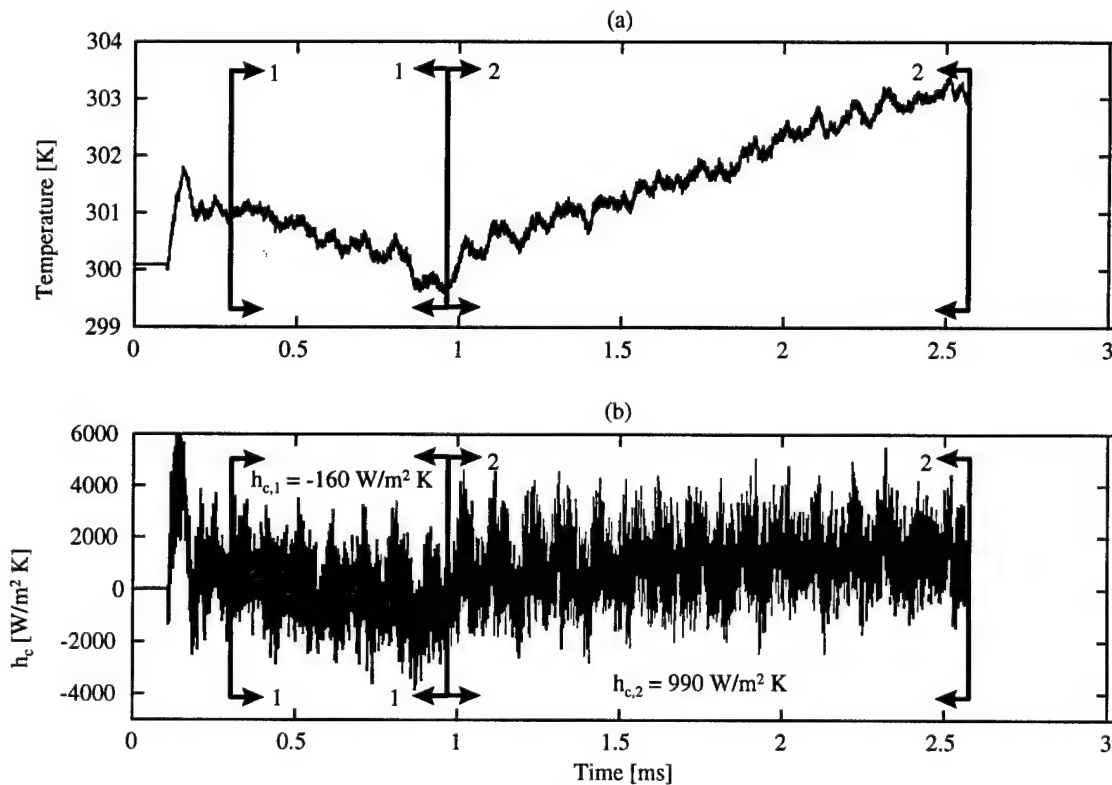
Figure 4.3 Representative Wet Run Results. Run 28, Thermocouple Station 2, $P_o = 2.1$ MPa, $T_o = 830$ K

34

To validate the explanation in the previous paragraph for the observed slope change in the temperature curves, the dry-out effect in region two was analyzed. $h_{c,2}$ was compared to h_u for runs of corresponding stagnation conditions. For each stagnation condition, $h_{c,2}$ was within 20% of h_u. This strengthens the argument that the effects of cooling are negligible in region two, and indicates there are probably some unknown effects of the residual water deep inside the wall. One exception to this occurred at thermocouple station three at a stagnation pressure of 2.0 MPa. In this case, $h_{c,2}$ was 65% less than h_u. This probably indicates residual effects of the water remaining deep inside the wall are more significant for lower pressures at locations farther downstream. Still, for purposes of this analysis, data in region two are not of interest, and the remainder of this report will focus on the data in region one, where cooling effects are prominent. From this point forward, the convection coefficient in region one, $h_{c,1}$, will be abbreviated as h_c.

The convection coefficients at Stations two and three for all wet runs are plotted in Figs 4.4 and 4.5. In each graph, the solid line represents the averages of these points for each stagnation condition, which are also given in Table 4.2. The dashed line is a repeat of Fig 4.2, shown again here to visualize the effect of the cooling relative to the uncooled conditions. It is important to note as the stagnation pressure was increased, the difference between the two slopes in the wet run temperature curves became significantly less distinct than that of Fig 4.3(a), making it difficult at times to find the point of transition from region 1 to region 2. The relatively large standard deviations seen in Table 4.2 are likely a result of this problem as well as the uncertain repeatability of the nozzle wetting procedure. Great care was taken to wet the nozzle as consistently as possible, but there was no feasible method available to measure the amount of water applied.
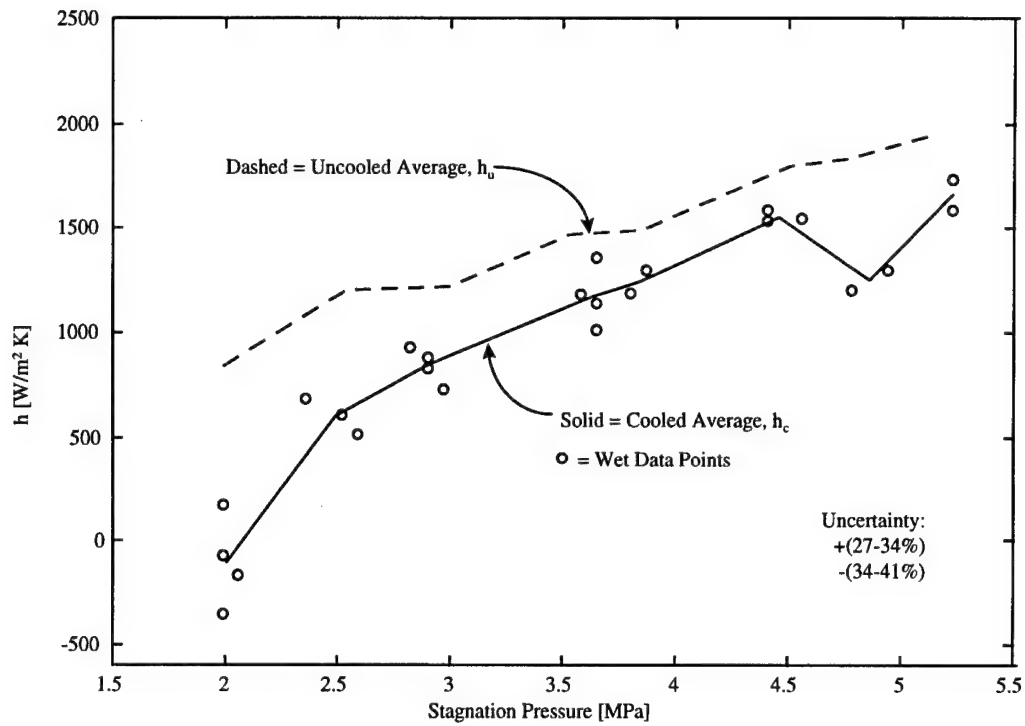
Figure 4.4 Convection Coefficient, Thermocouple Station 2 (Wet Nozzle)
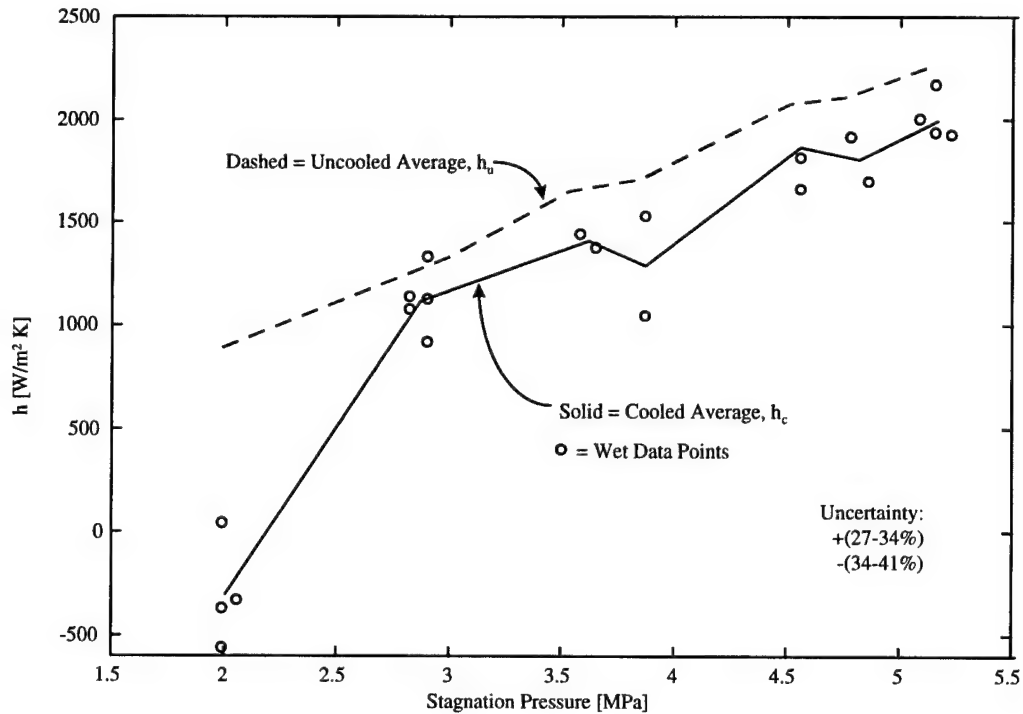
Figure 4.5 Convection Coefficient, Thermocouple Station 3 (Wet Nozzle)

Table 4.2 Convection Coefficient (Wet Nozzle)

P_o [MPa]	Station 2		Station 3	
	h [W/m² K]	Std Dev	h [W/m² K]	Std Dev
2.01	-100	200	-300	300
2.49	600	100	no data	-
2.89	800	200	1100	100
3.63	1200	100	1400	100
3.85	1200	100	1300	100
4.49	1600	100	1900	200
4.84	1300	300	1800	100
5.17	1700	100	2000	100

The convection coefficient information in Figs 4.4 and 4.5 is shown again in Fig 4.6 as a cooling effectiveness, η, defined as the percent reduction from the dry case.

$$\eta = 100\left(1 - \frac{h_c}{h_u}\right)$$

$$(4.4)$$

The effectiveness of liquid transpiration cooling demonstrates a nonlinear, inverse relation to
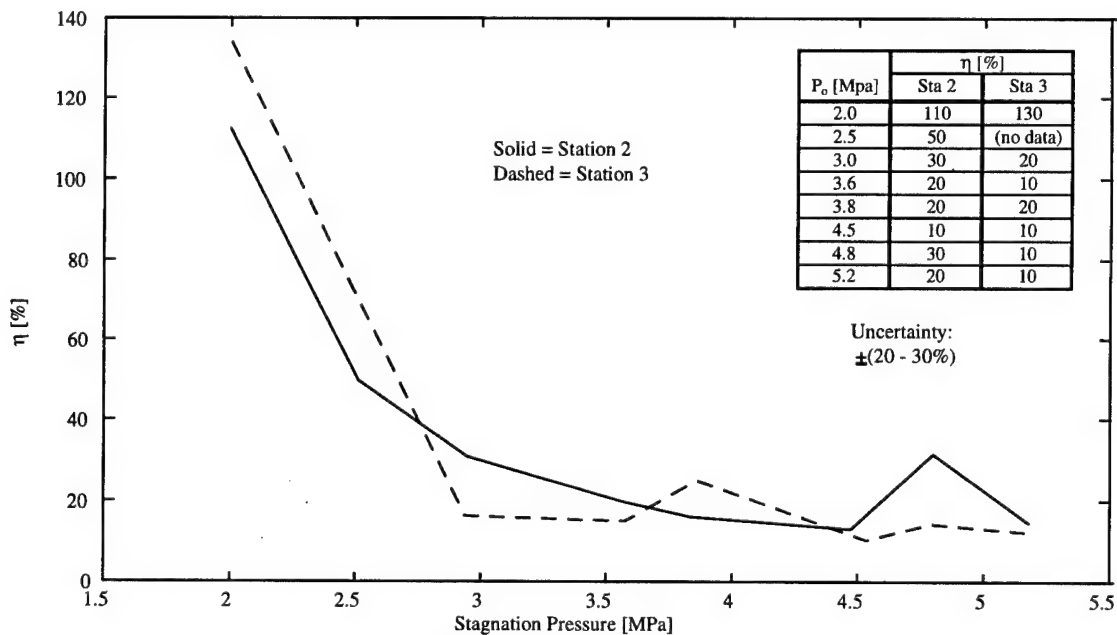
Figure 4.6 Cooling Effectiveness

stagnation pressure. This inverse relationship with stagnation conditions is primarily explained by the energy balance described by Eq (2.10). Two principle causes of the inverse relationship are identified from this energy balance. First, coolant mass flux is expected to be inversely proportional to pressure as discussed in Section 2.2. With decreasing coolant mass flux, Eq (2.11) dictates the heat absorbed by evaporation, q_{evap}", will also decrease. Therefore, as pressure is increased, q_{evap}" decreases, and according to Eq (2.10), more of the total heat transferred must go to the nozzle wall. Second, assume q_{evap}" were constant with pressure (not true, but conservative for this discussion). As the stagnation pressure of the primary flow increases, so does the stagnation temperature, and hence the total heat transferred from the hot gas. According to Eq (2.10), if q_{evap}" were constant, this excess heat must be transferred to the nozzle wall. Essentially, *as the stagnation pressure increases, the total heat transferred increases and the heat absorbed by evaporation decreases. Both of these effects cause an increase in the heat transferred to the nozzle wall.*

At the lowest pressure tested, the resulting effectiveness, $\eta > 100\%$, indicates the liquid transpiration cooling not only prevented the heat transfer to the nozzle wall, but actually *removed additional heat*, resulting in a surface temperature *lower* than initial. This effect can be seen clearly in Fig 4.3(a). At stagnation pressures above 3 MPa, cooling effectiveness virtually leveled off around 20% at station two and 10% at station three.

The liquid transpiration cooling appears to compare well with transpiration cooling using gasses as coolant. The tests using air studied different test conditions, so this comparison is presented only as a *very rough* comparison between liquid and gas coolants. Lenertz (1994) and Chen (1995) experimented with transpiration cooling using the AFIT Low Pressure Shock Tube to generate stagnation conditions for a 2-D Mach 2 nozzle fitted with a porous stainless steel

wall. This porous wall had a plenum chamber on the back side. Varying the air coolant pressure in this chamber allowed the coolant flow rate to be varied. Wall surface temperature data was taken and used to calculate convection heat transfer coefficients, as described in Chapter 2. Stagnation pressure for both of these experiments was held constant near 0.5 MPa throughout testing. This is below the lowest stagnation pressure studied here, but the trend in Fig 4.6 indicates liquid transpiration cooling may be highly effective (potentially over 100%) at these low pressures. At the highest coolant flow rates studied, Lenertz and Chen achieved cooling efficiencies of 14% and 40%, respectively. Still, the benefits of choosing a liquid transpiration coolant over a gas are expected to diminish as pressure is increased.

V. Conclusions and Recommendations

5.1 Conclusions

In an effort to aid in identifying improved design possibilities of rockets, an experiment was performed to demonstrate the effects of liquid transpiration cooling on the heat transfer to the diverging portion of a porous nozzle wall over a wide range of flow stagnation conditions. The goal was to broaden the knowledge base in this field, bringing the rocket design community one step closer to overcoming nozzle material thermal limitations, which ultimately will lead to the design of more powerful rockets than those in use today.

This method of cooling showed outstanding potential at low stagnation pressures, demonstrating a cooling effectiveness of up to 130% for a stagnation pressure of 2 MPa. The cooling effectiveness diminished with increasing stagnation pressures, nearly leveling off between 10 and 20% for stagnation pressures between 3 and 5.2 MPa. This inverse relationship with stagnation conditions is due to the fact that the total heat transferred increased with pressure while the coolant mass flux decreased. With these two effects, conservation of energy required the heat transferred to the nozzle wall to increase.

A rough comparison between this and other tests shows liquid transpiration cooling to compare well with gas transpiration cooling. Previous testing of gas transpiration cooling at a stagnation pressure of 0.5 MPa demonstrated cooling effectiveness to be as high as 40%. The stagnation conditions of this experiment were much higher, but extrapolating the results to lower pressures indicates liquid transpiration cooling could potentially exceed 100% cooling effectiveness at a stagnation pressure of 0.5. It was expected that the use of a liquid coolant would be an improvement over gas coolant, because liquids offer the same boundary layer

cooling and enhancement effects as gasses, but also introduce the evaporation process to absorb additional energy. This additional benefit is expected to taper off with higher pressures.

It must be noted that the results of this study may not be directly applicable to nozzle cooling systems with forced liquid coolant flow. The coolant was not replenished during testing, so the gas-liquid interface was moving as coolant evaporated (see Fig 2.1). In practical applications with forced coolant flow, it is expected the gas-liquid interface would be stationary during steady state conditions. The impact this effect may have on the results presented in this report is not known.

5.2 Recommendations

Five recommendations for future experimental research of liquid transpiration cooling are made as a result of lessons learned during this research effort.

First, as discussed in Section 1.4, this experiment was unable to obtain useful data near the throat. Peak heat flux occurs near the throat of a nozzle (Hill and Peterson, 1992:550), therefore the true measure of a cooling system is how well it operates in the throat region (Landis 1995:1). Therefore, future experiments should incorporate a porous nozzle wall region that begins upstream of the throat, so that meaningful data can be collected at or near the throat.

Second, this experiment demonstrated that liquid from a saturated wall evaporates too quickly to provide good wet nozzle run times. A forced coolant feed system is necessary. To incorporate this, the problem of puddling must be overcome, so a facility is needed that will provide longer run times than that of a shock tunnel to achieve steady state conditions. Ideally, such a facility should also generate high stagnation pressures and temperatures. Advantages of a facility with these capabilities include more data per run, improved consistency for wet nozzle runs, and measurable liquid coolant consumption.

41

Third, the test section should be positioned vertically with the exhaust flowing downward. This was demonstrated by a graduate level heat transfer class at the Air Force Institute of Technology to be an effective way to provide forced blowing of a liquid through the porous material, avoiding the problem of puddling. It also allowed the measurement of the mass flow of coolant by measuring the volumetric influx , collecting drops falling out, and assuming $m_{evap} = m_{in} - m_{out}$ (Bowman, et al, 1997). This may allow liquid transpiration cooling to be effectively studied using a shock tunnel, and may be an alternative solution to the second recommendation above. Though worth checking into, modification of existing facilities to incorporate a vertical test section may be costly or impractical.

Fourth, more testing is required at higher stagnation pressures (above 3.0 MPa) to better evaluate the effectiveness of liquid transpiration cooling at pressures required for high performance rockets.

Finally, the use of coaxial thermocouples proved easy with excellent results; their use is highly recommended over thin film resistance thermometers (heat flux gauges) used by previous researchers. Chadwick (1997:3) indicates the accurate calibration of thin film resistance thermometers is the key to obtaining quality heat transfer data. He also states the electrical resistance must be carefully monitored during testing. Lenertz (1994:49) describes the heat flux gauges as "fragile and difficult to calibrate. From a total of twelve gauges acquired during [his] study, only two remained operational at the end." In sharp contrast, the coaxial thermocouples need no calibration and their substrate thermophysical properties are well determined, allowing good heat transfer calculations. They are also exceptionally durable; unlike the heat flux gauges, they are not exposed to currents capable of destroying them, and damage to the sensing surface can be easily repaired. Moreover, the sensing surface area is significantly smaller, allowing them to be placed flush with contoured surfaces without disrupting the flow over the surface.

## Appendix A - Summary of Shock Tunnel Runs

Run	Date/Time	Test Condition Group (1-8)	Dry/Wet Nozzle	Driver Pressure [psig]	Stagnation Pressure, P_o [Mpa]	Stagnation Temperature, T_o [K]	Purpose	Comments	h [W/m² K] (Station 2)	h [W/m² K] (Station 3)
1	2 May/1521	N/A	N/A	~100	unk	unk	Setup	Thin Diaphragm		
2	2 May/1538	N/A	N/A	~100	0.4	unk	Setup	Thin Diaphragm		
3	5 May/1419	N/A	N/A	~100	unk	unk	Setup	Thin Diaphragm		
4	5 May/1520	N/A	N/A	~85	0.3	unk	Setup	Thin Diaphragm		
5	29 May/1619	N/A	N/A	294	1.3	unk	Setup			
6	30 May/1416	N/A	N/A	307	1.3	unk	Setup			
7	30 May/1521	N/A	N/A	630	unk	unk	Setup			
8	3 Jun/1345	N/A	N/A	575	2.3	unk	Setup			
9	3 Jun/1438	N/A	N/A	928	unk	unk	Setup			
10	5 Jun/1603	N/A	N/A	995	unk	unk	Setup			
11	30 Jun/1628	N/A	N/A	896	4.4	unk	Setup			
12	30 Jun/1701	N/A	N/A	1191	5.4	unk	Setup	Xducer Limit Exceeded		
13	30 Jun/1815	N/A	N/A	1191	5.4	unk	Setup	Xducer Limit Exceeded		
14	1 Jul/0851	N/A	N/A	1499	6.3	unk	Setup	Xducer Limit Exceeded		
15	2Jul/1530	N/A	N/A	1000	4.9	unk	Setup	Xducer Limit Exceeded		
16	1 Aug/1600	N/A	D	2003	unk	unk	Setup	New Xducer Installed		
17	4 Aug/1017	N/A	D	1003	unk	unk	Setup			
18	4 Aug/	N/A	W	1003	unk	unk	Testing	Destroyed Test Section		
19	26 Aug/	N/A	D	400	unk	unk	Testing	Acquisition Problems		
20	26 Aug/	N/A	D	397	unk	unk	Testing	Acquisition Problems		
21	26 Aug/	N/A	D	397	unk	unk	Testing	Acquisition Problems		
22	26 Aug/1614	1	D	403	2.06	755	Testing	Bad Data		
23	29 Aug/1505	1	D	403	1.99	837	Testing		788	867
24	29 Aug/1525	1	D	400	2.06	850	Testing		869	931
25	29 Aug/1605	1	W	402	1.99	826	Testing		172	47
26	29 Aug/1630	1	W	398	1.99	825	Testing		-68	-371
27	29 Aug/1655	1	W	397	1.99	848	Testing		-352	-559

Run	Date/Time	Test Condition Group (1-8)	Dry/Wet Nozzle	Driver Pressure [psig]	Stagnation Pressure, P_o [Mpa]	Stagnation Temperature, T_o [K]	Purpose	Comments	h [W/m² K] (Station 2)	h [W/m² K] (Station 3)
28	30 Aug/2012	1	W	402	2.06	828	Testing		-162	-330
29	2 Sep/1737	3	D	650	2.82	845	Testing	Bad Data		
30	2 Sep/1835	3	D	646	3.05	1021	Testing		1204	1292
31	2 Sep/1917	3	D	650	3.12	1034	Testing		1197	1319
32	2 Sep/1937	3	W	647	2.97	998	Testing		730	
33	2 Sep/2001	3	W	650	2.9	960	Testing			1127
34	2 Sep/2022	3	W	660	2.9	962	Testing		831	918
35	3 Sep/1413	4	D	797	3.43	1050	Testing		1510	1714
36	3 Sep/1439	4	D	792	3.58	1086	Testing		1447	1613
37	3 Sep/1530	4	D	800	3.58	1078	Testing		1444	1629
38	3 Sep/1601	4	W	798	3.65	1107	Testing		1011	
39	3 Sep/1621	4	W	797	3.65	1104	Testing		1138	
40	3 Sep/1647	4	W	798	3.58	1077	Testing		1184	1441
41	4 Sep/1321	5	D	946	3.8	1137	Testing		1428	1698
42	4 Sep/1341	5	D	951	3.87	1142	Testing		1489	1706
43	4 Sep/1408	5	D	948	3.87	1137	Testing		1551	1733
44	4 Sep/1505	5	W	948	3.8	1121	Testing		1189	
45	4 Sep/1527	5	W	948	3.65	1091	Testing		1356	1372
46	4 Sep/1559	5	W	946	3.87	1128	Testing		1300	1528
47	9 Sep/1347	1	D	402	1.92	807	Testing		857	872
48	9 Sep/1414	3	D	646	2.82	942	Testing		1267	1388
49	9 Sep/1441	3	W	649	2.82	945	Testing			1076
50	9 Sep/1503	3	W	655	2.82	937	Testing		928	1139
51	9 Sep/1529	5	W	951	3.87	1122	Testing		1046	
52	12 Sep/1447	2	D	499	2.52	890	Testing		1129	1224
53	12 Sep/1505	2	D	499	2.52	892	Testing		1389	1261
54	12 Sep/1521	2	D	504	2.59	915	Testing		1098	1268
55	12 Sep/1538	2	W	502	2.36	848	Testing		685	
56	12 Sep/1555	2	W	501	2.59	924	Testing		515	
57	12 Sep/1614	2	W	504	2.52	890	Testing		610	
58	12 Sep/1638	2	W	504	2.21	648	Testing	Bad Data		
59	12 Sep/1657	3	W	650	2.9	947	Testing		881	1331

| Run	Date/Time	Test Condition Group (1-8)	Dry/Wet Nozzle	Driver Pressure [psig]	Stagnation Pressure, P_o [Mpa]	Stagnation Temperature, T_o [K]	Purpose	Comments	h [W/m^2 K] (Station 2)	h [W/m^2 K] (Station 3)
60	15 Sep/1555	6	D	1102	4.71	1282	Testing		1753	2041
61	15 Sep/1650	6	D	1102	3.72	888	Testing	Bad Data		
62	15 Sep/1715	6	D	1101	4.33	1180	Testing		1836	
63	15 Sep/1817	6	D	1102	4.48	1220	Testing		1801	2099
64	15 Sep/1851	6	W	1098	4.56	1240	Testing			1664
65	15 Sep/1913	6	W	1101	4.56	1230	Testing		1546	1815
66	15 Sep/1937	6	W	1102	4.41	1207	Testing		1583	
67	15 Sep/1957	6	W	1102	4.41	1197	Testing		1532	
68	16 Sep/1605	7	D	1250	4.78	1278	Testing		1781	2071
69	16 Sep/1628	7	D	1255	4.86	1300	Testing		1725	2031
70	16 Sep/1650	7	D	1254	4.63	1231	Testing		1992	2223
71	16 Sep/1722	7	W	1247	4.86	1298	Testing			1698
72	16 Sep/1744	7	W	1255	4.94	1311	Testing		1297	
73	16 Sep/1806	7	W	1257	4.78	1264	Testing			1916
74	16 Sep/1832	7	W	1246	4.78	1281	Testing		1204	
75	18 Sep/1352	8	D	1402	5.16	1328	Testing		1937	2249
76	18 Sep/1418	8	D	1400	5.23	1343	Testing		1910	2167
77	18 Sep/1442	8	D	1400	5.09	1294	Testing		2013	2383
78	18 Sep/1506	8	W	1403	5.16	1309	Testing			2170
79	18 Sep/1533	8	W	1405	5.23	1326	Testing		1586	1925
80	18 Sep/1554	8	W	1398	5.16	1312	Testing			1935
81	18 Sep./1619	8	W	1395	5.09	1297	Testing			2006
82	18 Sep/1637	8	W	1402	5.23	1325	Testing		1735	1925

Thermocouple Station 2 – Useable Data Sets
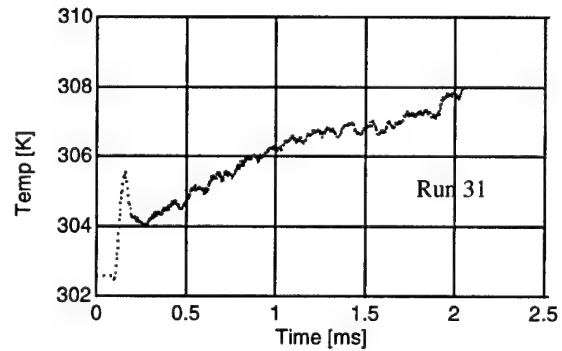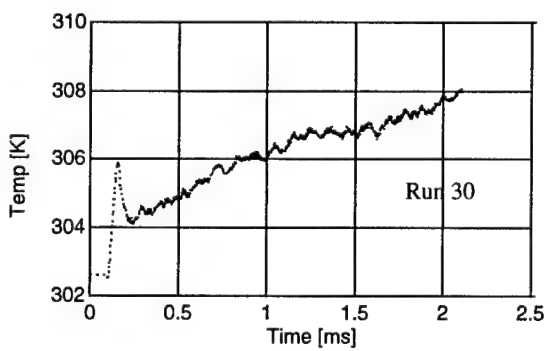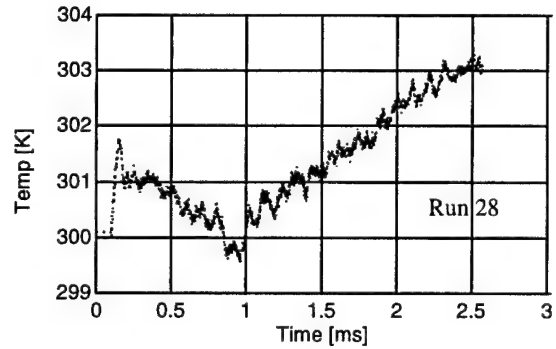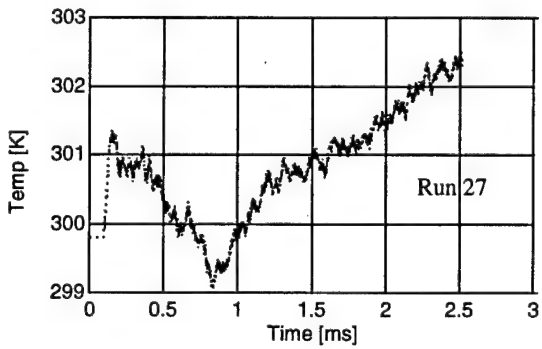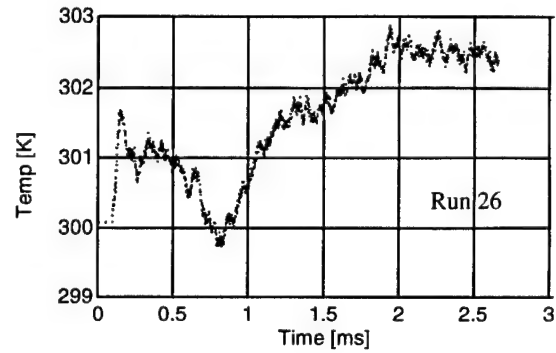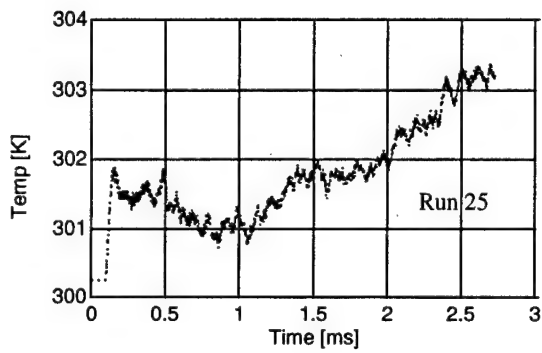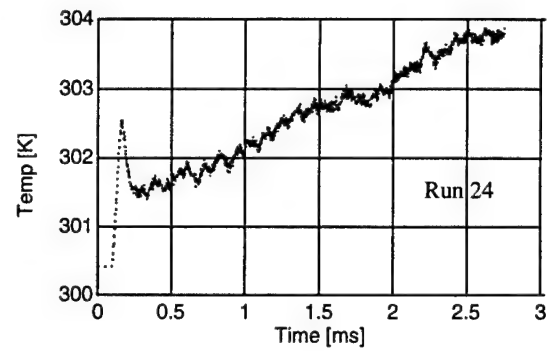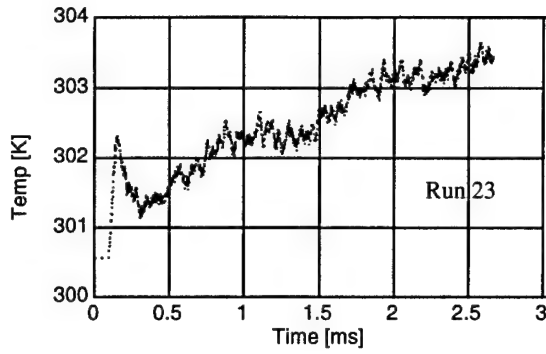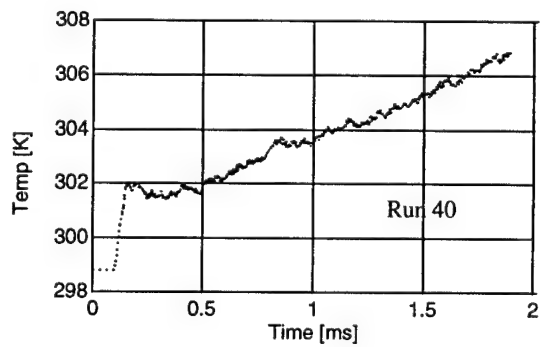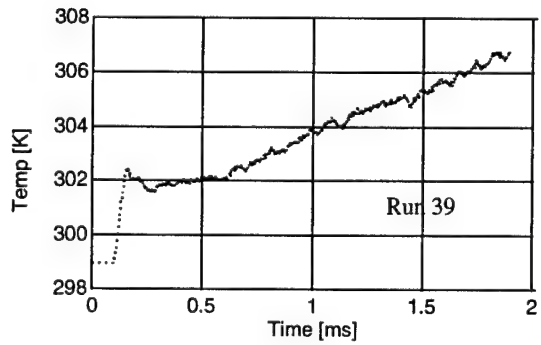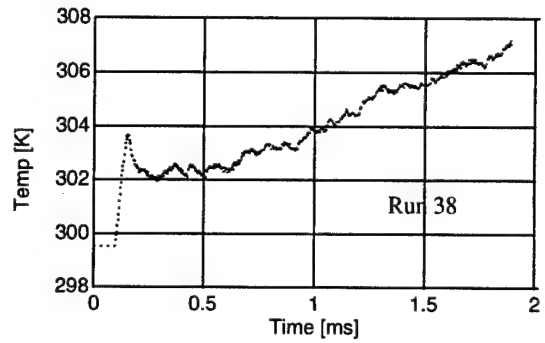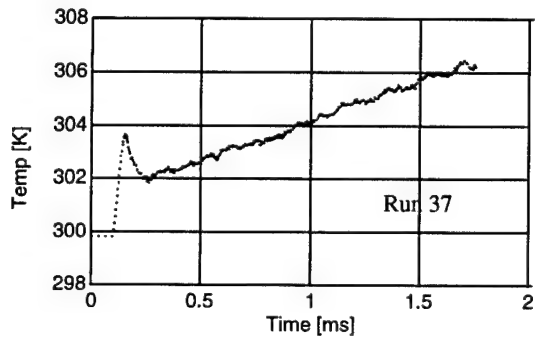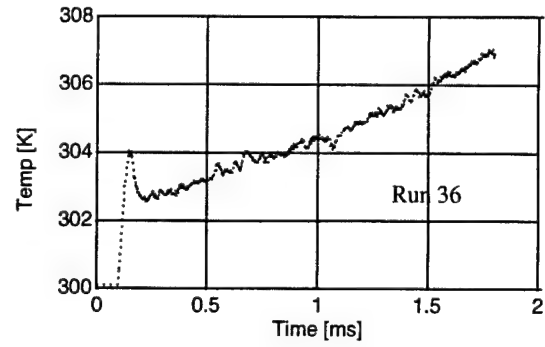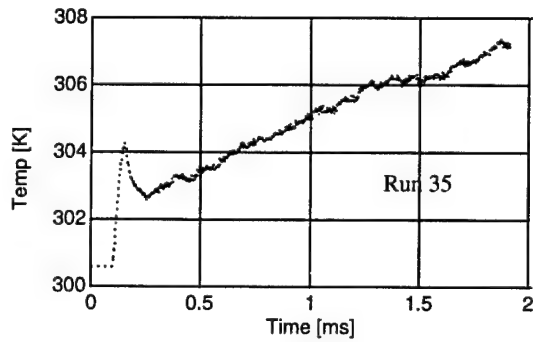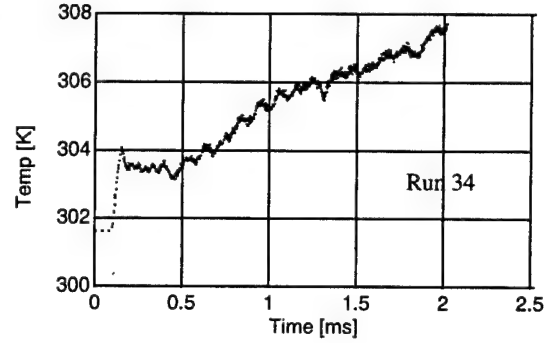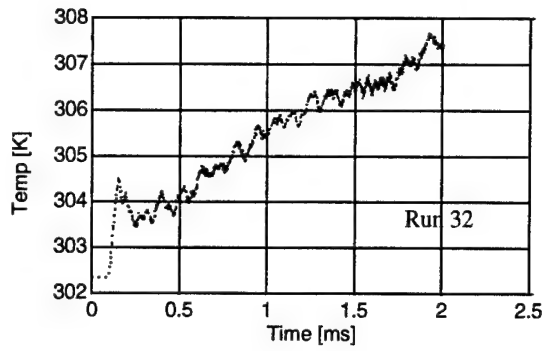
Thermocouple Station 2 – Useable Data Sets

Thermocouple Station 2 – Useable Data Sets

Thermocouple Station 2 – Useable Data Sets

Thermocouple Station 2 – Useable Data Sets

Thermocouple Station 3 – Useable Data Sets

Thermocouple Station 3 – Useable Data Sets
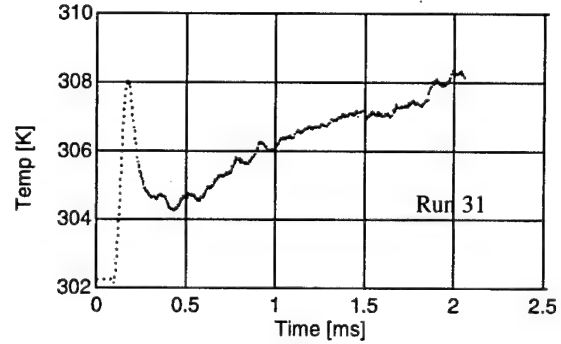
Thermocouple Station 3 – Useable Data Sets
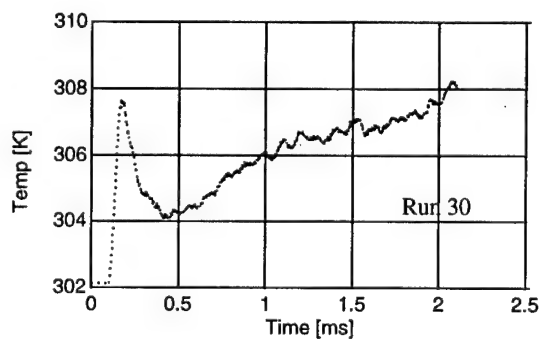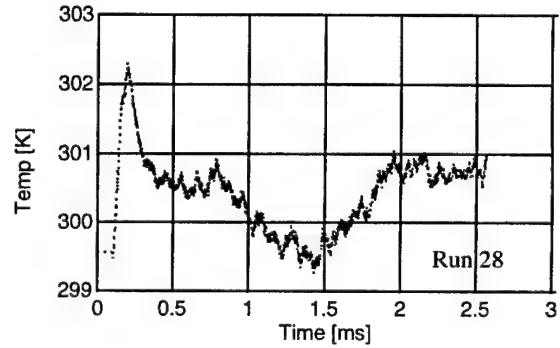
Thermocouple Station 3 – Useable Data Sets

Thermocouple Station 3 – Useable Data Sets

57

Thermocouple Station 3 – Useable Data Sets

58
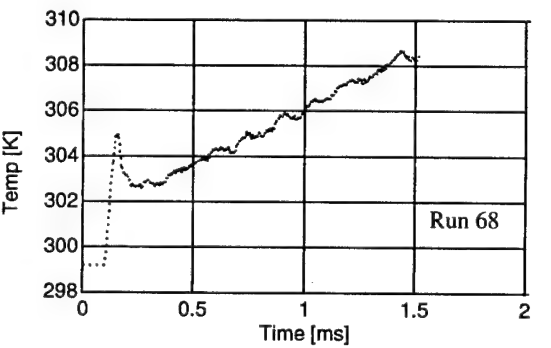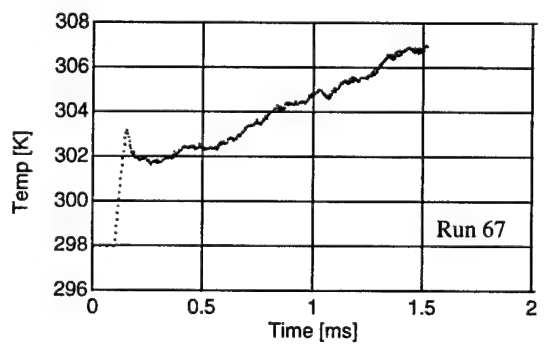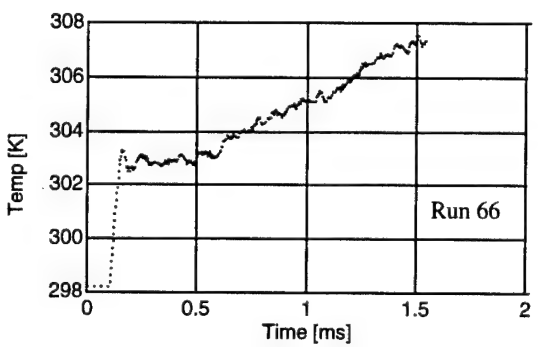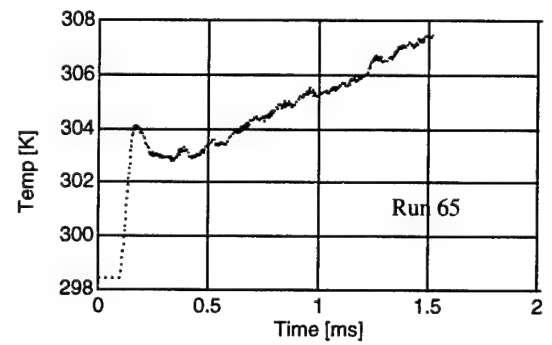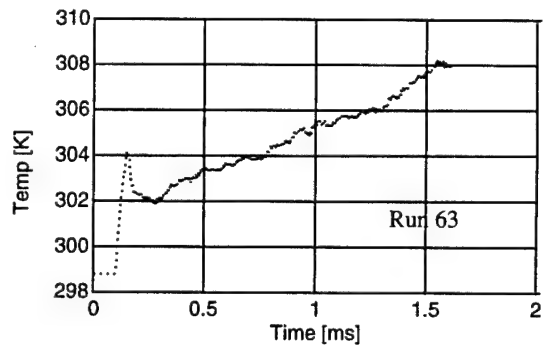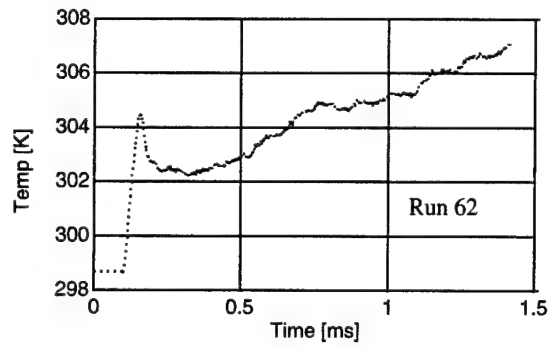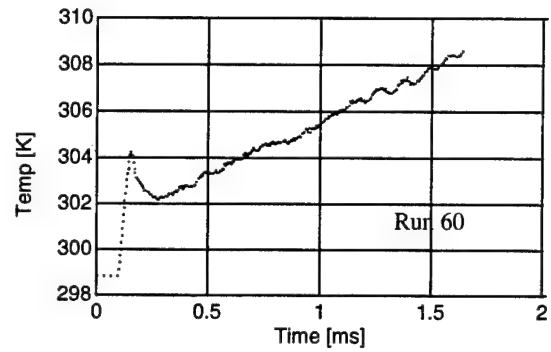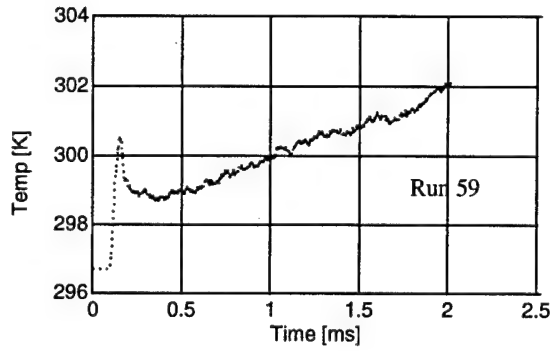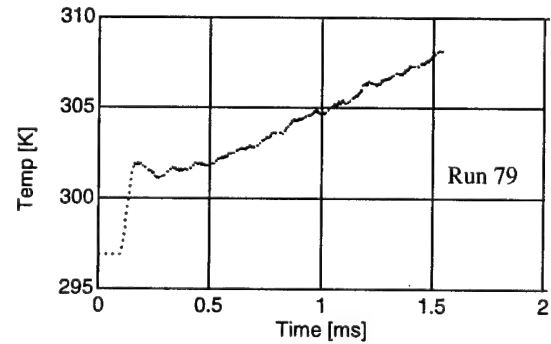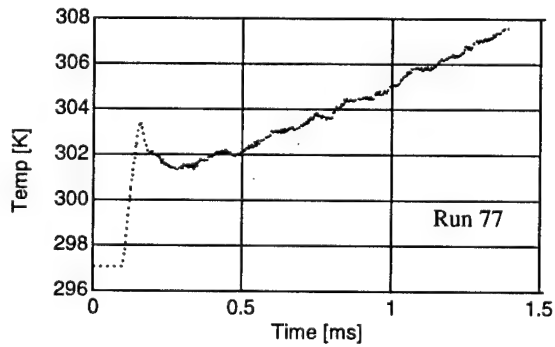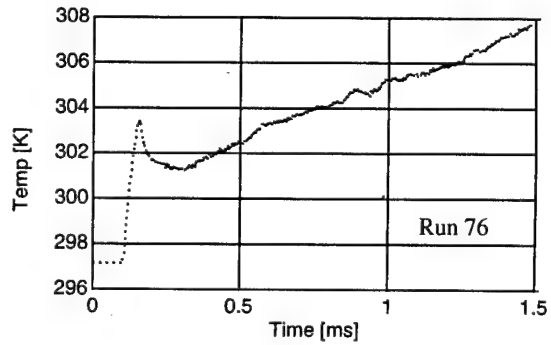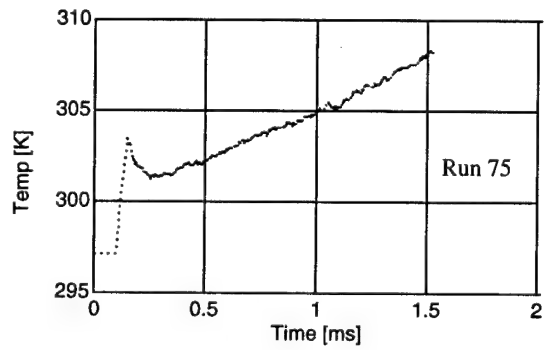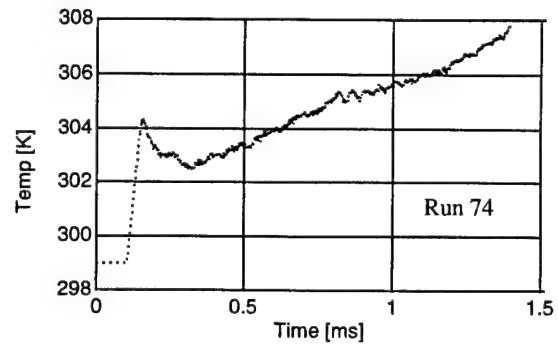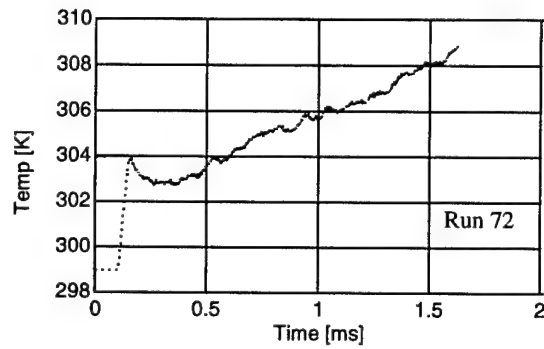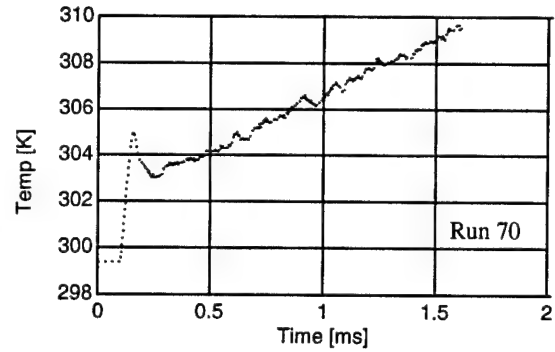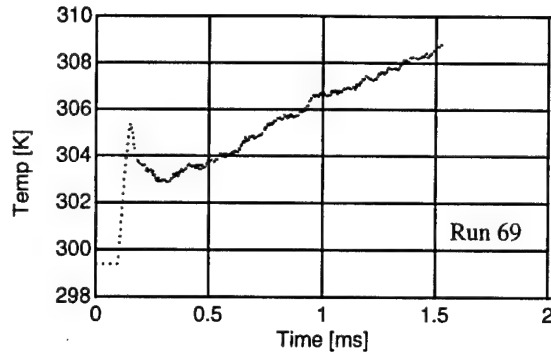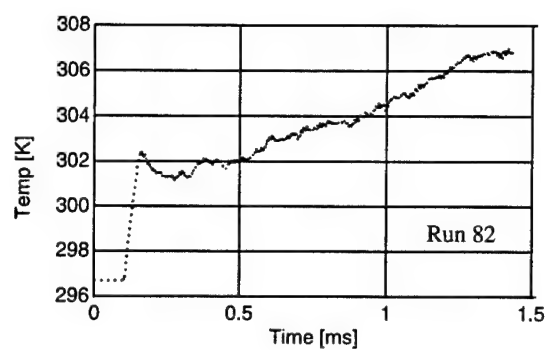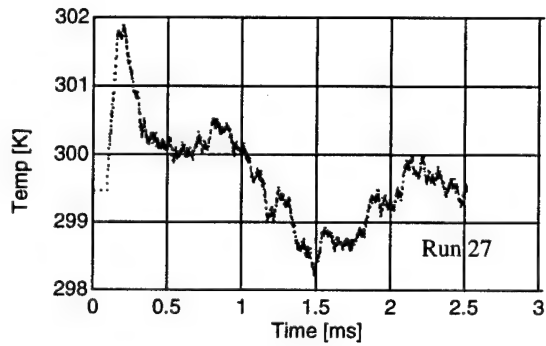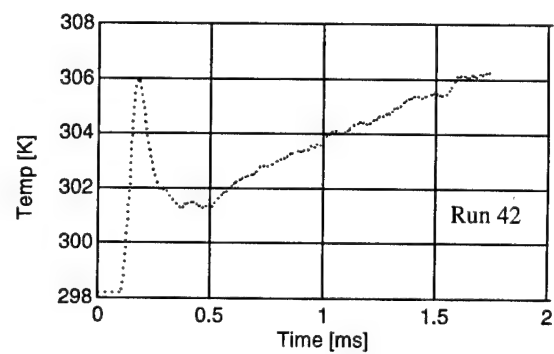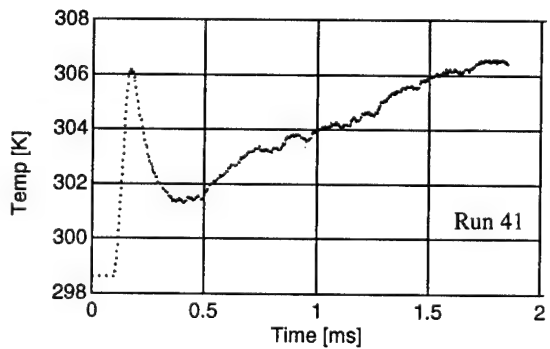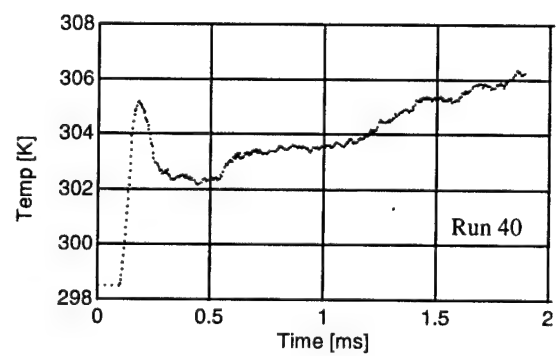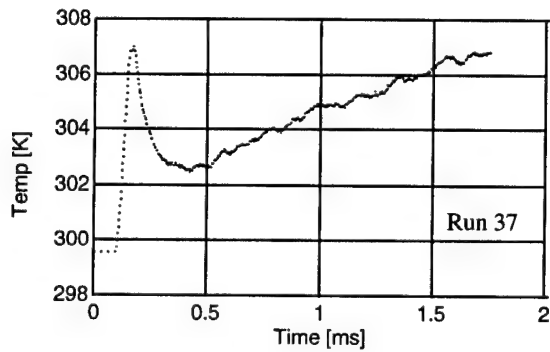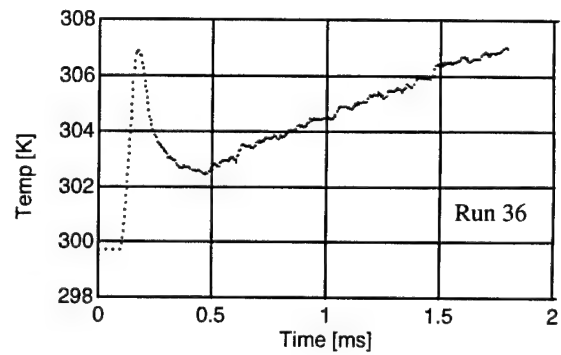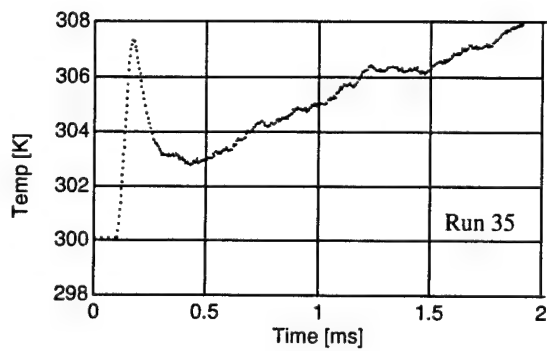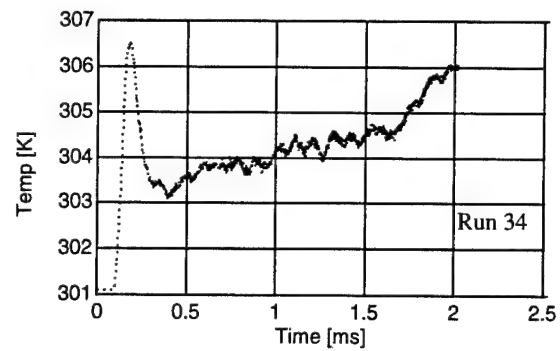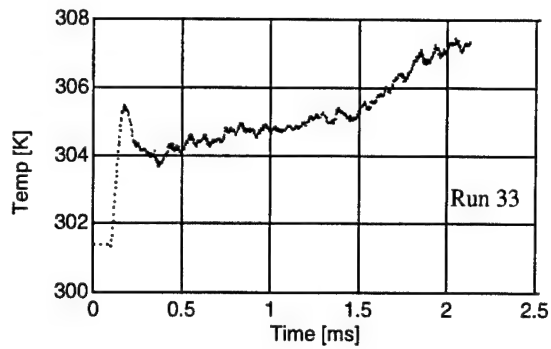
Appendix B - Computer Programs

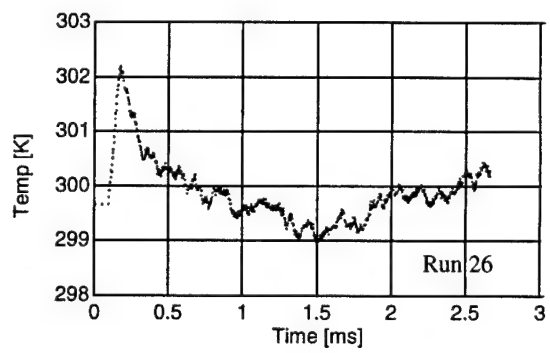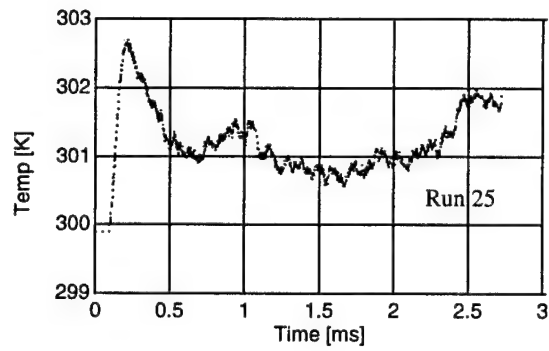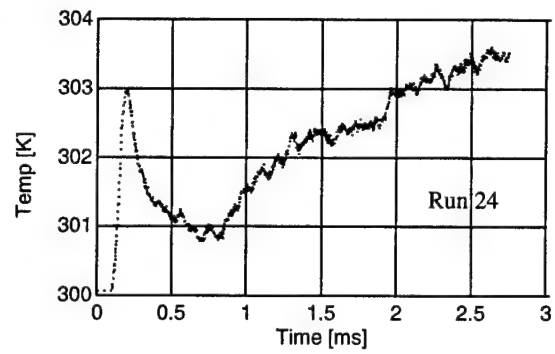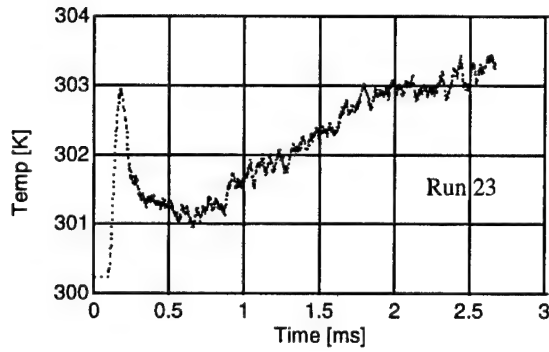This section contains the computer codes used to analyze data as described in Section 3.6. Programs included here are the Matlab programs *reduce.m*, *viewtemp.m*, *convec.m*, and *tester.m*. The codes include their own introduction and explanations where necessary.

% **reduce.m**

% This program inputs a data file that has been modified in
% Excel to be a text file with one column of Thermocouple
% voltage data. The time increment for the data must be
% one microsecond. It then converts the voltages to Kelvin,
% filters it, and plots the temperature history. The user
% then looks at the plot and is prompted to input information
% to determine the time of shock passage over the thermocouple
% station. All data points before the shock are averaged and
% this value is called the initial temperature. All data
% points prior to the shock are reset to this value and the
% data set is cropped to only include 100 points (0.1 ms)
% before the shock. The end of the data set is also cropped
% at the end of steady state period. This new filtered and
% reduced data set is saved to a new text file to be used by
% the program convec.m.

% ----------------- CLEAR ALL VARIABLES --------------------

```
check = input('Do you wish to CLEAR? (y/n) ','s');
if check == 'y';
        clear
end
```

% ------------------ LOAD DATA FILE ------------------------

% All data files are saved in the format rXXXc3X.txt, where
% the X's indicate the run number and thermocouple station.

```
run = input('Enter the 3-digit run #: ','s');
sta = input('Which Thermocouple Station? (1, 2, 3, or 4) ');

if sta == 1;
        filename = ['r',run,'c3a']
elseif sta == 2;
        filename = ['r',run,'c3b']
elseif sta == 3;
        filename = ['r',run,'c3c']
else
        filename = ['r',run,'c3d']
end

filenamedottxt = [filename,'.txt'];

eval(['load ' filenamedottxt]);
temp = eval(filename);
```

% ---------------------- INPUTS ----------------------------

```
t_ent=input('Time of shock at NOZ ENTR xducer [microsec]: ');
t_end = input('SS END Time from Data Sheet [microsec]: ');
```

```
% ---------------- TIME CALCULATIONS -----------------------

% The following times are in microseconds

   points = size(temp,1)            % Total length of data
   dur = t_end - t_ent;             % Duration from shock to SS End

% ------- CONVERT THERMOCOUPLE VOLTAGE TO TEMPERATURE -------

% Uses the function given on page A7 of the Thermocouple
% Reference Tables, Omega Engineering, Inc., 1993.
% T(E) where E is in volts and T is in Kelvin.

   c0 =  273.15;
   c1 =  1.7057035e-2;
   c2 = -2.3301759e-7;
   c3 =  6.5435585e-12;
   c4 = -7.3562749e-17;
   c5 = -1.7896001e-21;
   c6 =  8.4036165e-26;
   c7 = -1.3735879e-30;
   c8 =  1.0629823e-35;
   c9 = -3.2447087e-41;

   for j = 1:points;
         E = temp(j);
         E = E*1e6;          % Convert to microvolts

         T(j) = c0 + c1*E + c2*E^2 + c3*E^3 + c4*E^4 + .....
                c5*E^5 + c6*E^6 + c7*E^7 + c8*E^8 + c9*E^9;
   end;

   T = T';           % Convert row to a column vector

% ---------------------- FILTER --------------------------

% Each point is averaged with the 25 before and 25 after.  The
% first 25  points and last 25 points are left as is.

   for N = 1:25;
         Tfil(N) = T(N);
   end

   for N = 26:(points-25.);
         Tfil(N) = 0.;
         for n = N-25:N+25;
                 Tfil(N) = Tfil(N) + T(n);
         end
         Tfil(N) = Tfil(N)/51.;
   end

   for N = (points-24):points;
         Tfil(N) = T(N);
```

```
        end

    Tfil = Tfil';                % Convert row to a column vector

% ----------------- GENERATE TIME VECTOR --------------------

    t(1) = 0.;
    for j = 2:points;
            t(j) = t(j-1) + .000001;
    end

    t = t';              % Convert row to a column vector

% ------------------------- PLOTS -------------------------

    figure(1)
    plot(t,Tfil,'r')
    grid

% ----------------- CONTINUE OR TERMINATE --------------------

    cont = input('Find the shock time? (y/n): ','s');
    if cont == 'n';
            error('Program terminated by user -- no actual error.')
    end

% ------------------ FIND THE SHOCK TIME --------------------

% User inputs based on figure 1:

    starttime = input('Time to start check [microsec]: ');
    trigger = input('Trigger Temp [K]: ');

% Flag the data point, m, where the temp first exceeds the trigger
% temp.

    for m = starttime:points;
            if Tfil(m)>trigger;
                    break
            end;
    end;
    m

% Plot a close-up of the data points near m to the screen.

    j = 0;
    for n = m-25:m+5;
            j = j + 1;
            t_close(j) = n;
            Tfil_close(j) = Tfil(n);
    end;

    figure(2)
```

```
plot(t_close,Tfil_close,'y+')
grid
```

% User reviews the plot and determines the shock arrival time.

```
shocktime = input('Shock Time [microsec]: ');
```

% ---------------- FIND MEAN INITIAL TEMP -----------------

```
Ti = 0.;
for m = 1:shocktime;
        Ti = Ti + T(m);
end
Ti = Ti / shocktime
```

% Reset filtered temp prior to shock to Ti

```
for n = 1:shocktime;
        Tfil(n) = Ti;
end
```

% ----------- CREATE NEW TEMPERATURE FILE ------------------

% Crop the ends of the temperature history

```
for m = 1:(dur + 100);
        tnew(m) = t(shocktime-100+m);
        Tnew(m) = Tfil(shocktime-100+m);
end
```

```
tnew = tnew';
Tnew = Tnew';
```

```
save reduced Tnew -ascii
```

% ------------------------- PLOTS -------------------------

% Visual verification of reduction success.

```
figure(3)
plot(t,T,'g')
hold
plot(tnew,Tnew,'r')
hold
```

```
end
```

% viewtemp.m

```matlab
% ----------------- CLEAR ALL VARIABLES --------------------

check = input('Do you wish to CLEAR? (y/n) ','s');
if check == 'y';
        clear
end

% ------------------ LOAD DATA FILE -----------------------

filename = input('Data file name:  ','s');
filenamedottxt = [filename,'.txt'];
eval(['load ' filenamedottxt]);
temp = eval(filename);

points = size(temp,1);

% ----------------- GENERATE TIME VECTOR -------------------

% Time increment must be 1 microsecond.

t(1) = 0.;
for j = 2:points;
        t(j) = t(j-1) + .000001;
end

t = t';

% -------------------------- PLOTS ------------------------

figure(1)
plot(t,temp,'r')
grid

end
```

```
% convec.m

% This program uses numerical integration to calculate the
% convection heat transfer coefficient, h(t), from an input
% surface temperature history, T(0,t).  The temperature
% history must be one that has been filtered and reduced by
% the program reduce.m.

% It uses the same theory used by Lenertz and Chen for heat
% flux gauges.  The only difference is the medium used as a
% semi-infinite substrate.
% See Lenertz, eqs. 2.11, 17, & 19, p. 14-17.
% See Chen, eqs. 2.10, 14, & 23, p. 2-4 - 2-7.

% ----------------- CLEAR ALL VARIABLES --------------------

  check = input('Do you wish to CLEAR? (y/n) ','s');
  if check == 'y';
          clear
  end

% ------------------ LOAD DATA FILE ------------------------

% All data files are saved in the format rXXXc3XR.txt, where
% the X's indicate the run number and thermocouple station.

  run = input('Enter the 3-digit run #:  ','s');
  sta = input('Which Thermocouple Station? (1, 2, 3, or 4) ');

  if sta == 1;
          filename = ['r',run,'c3aR']
  elseif sta == 2;
          filename = ['r',run,'c3bR']
  elseif sta == 3;
          filename = ['r',run,'c3cR']
  else
          filename = ['r',run,'c3dR']
  end

  filenamedottxt = [filename,'.txt'];

  eval(['load ' filenamedottxt]);
  T = eval(filename);

  points = size(T,1);                            % Total length of data

% ---------------------- INPUTS ----------------------------

  t_up=input('Time of shock at UPSTREAM xducer [us]:  ');
  t_ent=input('Time of shock at NOZ ENTR xducer [us]:  ');

  Po1 = input('SS START measured noz entrance PRESS [psig]:  ');
  Po2 = input('SS END measured noz entrance PRESS [psig]:  ');
```

```matlab
wetrun = input('Wet run? (y/n):  ','s');

t_start = input('START Time from Result Sheet [us]:  ');

if wetrun == 'y';
        t_stop = input('Wet STOP Time from Result Sheet [us]:  ');
end
```

% ------------- CALCULATED FLOW PROPERTIES ------------------

% STAGNATION TEMPERATURE AND PRESSURE, To & Po

% Find incident shock Mach #

```matlab
Ti = T(1);
a = (1.4 * 8315./28.85 * Ti)^.5;              % [m/s]
        % Assumes the driven gas temp = initial wall temp


%v = 3.0925 / ((t_ent-t_up)/1000000.);       % [m/s] 25' driven
v = 1.5685 / ((t_ent-t_up)/1000000.);                   % [m/s] 20' driven
Mi = v/a;
```

% Theoretical (P5 & T5 in shock tube relations, given incident
% shock Mach #). Gamma = 1.4
% See Vlcek, eqs. 6 & 7, p. 9.

```matlab
P5 = 14.7 * (2.8*Mi^2 -.4) / 2.4 * (3.2*Mi^2 -.8) / (.4*Mi^2 +2);
T5 = Ti * (.8*Mi^2 + 1.6) * (3.2*Mi^2 -.8) / (5.76*Mi^2);
```

% Scale for actual (uses mean Steady State nozzle entrance pressure)

```matlab
Po = (Po1 + Po2)/2 + 14.7              % [psia]
To = T5 * (Po/P5)                      % [K]
```

% NOZZLE DIMENSIONS

```matlab
W = 1.499;                  % width [in] throughout
```

% Throat (station 0.0 in)

```matlab
Hstar = 0.355;    % height [in]
Astar = Hstar * W;        % area [in^2]
```

% Thermocouple 1 (sta 0.138 in)

```matlab
H1 = 0.372;
A1 = H1 * W;
AR1 = A1/Astar;                      % AR means Area Ratio
```

% Thermocouple 2 (sta 1.948 in)

```matlab
H2 = 1.038;
```

```
   A2 = H2 * W;
   AR2 = A2/Astar;

.  % Thermocouple 3 (sta 3.755 in)

   H3 = 1.371;
   A3 = H3 * W;
   AR3 = A3/Astar;

% Thermocouple 4 (sta 5.567 in)

   H4 = 1.509;
   A4 = H4 * W;
   AR4 = A4/Astar;

% NOZZLE FLUID PROPERTIES

% Throat Temperature and Pressure, Tstar & Pstar
% Uses the isentropic relations with gamma = 1.4
% See Hill & Peterson, eqs. 3.10 & 11, p. 70.

   Tstar = To/1.2;          % [K]
   Pstar = Po/1.2^3.5;              % [psia]

% Mach Numbers at Thermocouple Stations
% Uses the isentropic relation with gamma = 1.4
% See Hill & Peterson, eq. 3.15, p. 71.

   for M = 3.1:-.001:1.;
         AR = (((1.+.2*M*M)/1.2)^3.)/M;
         if AR > AR4;
               M4 = M;
         elseif AR > AR3;
               M3 = M;
         elseif AR > AR2;
               M2 = M;
         elseif AR > AR1;
               M1 = M;
         end;
   end;

% Freestream Gas (Static) Temperature at TC Stations
% Uses the isentropic relation with gamma = 1.4
% See Hill & Peterson, eq. 3.10, p. 70.

   T1 = To/(1.+.2*M1*M1);          % [K]
   T2 = To/(1.+.2*M2*M2);
   T3 = To/(1.+.2*M3*M3);
   T4 = To/(1.+.2*M4*M4);

% Adiabatic Wall Temperature, Taw, at TC Stations
% Uses the recovery factor, r, with gamma = 1.4
% See Lenertz, eqs. 2.7 & 8, p. 11-12.
```

```
% r = .91 for Mach numbers up to 4.
% See Hill & Peterson, p 546.


 r = 0.91;
 Taw1 = T1 * (1.+.2*r*M1*M1);   % [K]
 Taw2 = T2 * (1.+.2*r*M2*M2);
 Taw3 = T3 * (1.+.2*r*M3*M3);
 Taw4 = T4 * (1.+.2*r*M4*M4);

% SET VALUES FOR CORRECT STATION

 if sta == 1;
        M = M1;
        AR = AR1;
        Taw = Taw1;
 elseif sta == 2;
        M = M2;
        AR = AR2;
        Taw = Taw2;
 elseif sta == 3;
        M = M3;
        AR = AR3;
        Taw = Taw3;
 else
        M = M4;
        AR = AR4;
        Taw = Taw4;
 end


% ---------------- SUBSTRATE PROPERTIES --------------------


% Properties of Chromel at 300 K. Chromel is the material that
% makes up the tube of the coaxial thermocouples:
% Provided by the manufacturer, Medtherm Corp.

 rho = 8730.;               % [kg/m^3]
 c = 426.4;                 % [J/kg/K]
 k = 17.3;                  % [W/m/K]

 alpha = k/rho/c;  % [m^2/s]

 rck = rho*c*k;

% ------------- THEORETICAL h, USING BARTZ EQ --------------

% Dstar is a hydraulic diameter
% See Hill & Peterson, p. 549.


 Dstar = 2. * Astar / (Hstar + W) / 39.37;          % [m]


% Cstar, characteristic velocity, is simplified using an
% isentropic relation and gamma = 1.4
% See Hill & Peterson, eq. 11.8, p. 517, coupled with eq. 3.14,
```

```
% p. 71, simplifies to eq 11.9, p. 517.

  Cstar = sqrt(1.2^6 / 1.4 * 8315 / 28.85 * To);        % [m/s]

% Tw is the average wall temperature during SS

  Tw = 0.;
  for j = t_start:points;
          Tw = Tw + T(j);
  end;
  Tw = Tw / (points - t_start);

% sigma is simplified by omega = 0.6 for diatomic gasses.
% gamma = 1.4

  sigma1 = (Tw/2./To * (1.+.2*M*M) + .5)^.68;
  sigma2 = (1.+.2*M*M)^.12;
  sigma = 1./(sigma1 * sigma2);

% Throat radius of curvature, rc = 0.022 m.
% mu and Cp approximated by evaluating at To = 1400 K.
% See Keenan's Gas Tables.

  rc = .022;                % [m]
  mu = 510.e-7;             % [N-s/m^2]
  Cp = 1200.;               % [J/kg/K]

% Bartz equation, see Hill & Peterson, eq. 11.38, p. 550.
% Assume Pr = 0.7
% 1 psi = 6894.8 Pa.

  hbartz = .026/(Dstar*rc)^.1 * mu^.2*Cp/.7^.6;
  hbartz = hbartz * (Po*6894.8 / Cstar)^.8;
  hbartz = hbartz / AR^.9 * sigma

% ----------------- OBSERVED h(t) ------------------------

% GENERATE TIME VECTOR

  t(1) = 0.;
  for j = 2:points;
          t(j) = t(j-1) + .000001;
  end

  t = t';              % Convert row to a column vector

% See Lenertz, eqs. 17 & 19, p. 17.
% See Chen, eqs. 2.10 & 23, p. 2-4 - 2-7.

  h(1) = 0.;
  for J = 2:points;
          sum = 0.0;
          for j = 2:J;
```

69

```
                    term = (T(j)-T(j-1)) / .....
                            (sqrt(t(J)-t(j))+sqrt(t(J)-t(j-1)));
                    sum = sum + term;
            end
            q(J) = 2. * sqrt(rck/pi) * sum;
            h(J) = q(J) / (Taw - T(J));
    end

    h = h';              % Convert row to a column vector

% ----------------- CALCULATE AVG SS h ---------------------

    if wetrun == 'y';

            hwet = 0.;
            for j = t_start:t_stop;
                    hwet = hwet + h(j);
            end
            hwet = hwet/ (t_stop - t_start)

            hdry = 0.;
            for j = t_stop:points;
                    hdry = hdry + h(j);
            end
            hdry = hdry/ (points - t_stop)

    else

            hdry = 0.;
            for j = t_start:points;
                    hdry = hdry + h(j);
            end
            hdry = hdry/ (points - t_start)

    end

% -------- GENERATE THEORETICAL TEMPERATURE HISTORY ---------

% See Incropera & DeWitt, eq. 5.60, p. 239

    for j = 1:100;
            Ttheory(j)=Ti;
    end

    for j = 101:points;
            rhs1 = hdry * sqrt(alpha*t(j-100)) / k;
            rhs = 1 - exp(rhs1^2) * erfc(rhs1);
            Ttheory(j) = (Taw - Ti) * rhs + Ti;
    end

    Ttheory = Ttheory';              % Convert row to a column vector

% ---------------------- PLOTS ------------------------------
```

% Plot surface temperature and convection coef histories.

```
figure(1)
subplot(2,1,1)
plot(t,T,'w')
hold
if wetrun == 'y';
        plot(t(t_start),T(t_start),'wo')
        plot(t(t_stop),T(t_stop),'wo')
else
        plot(t(t_start),T(t_start),'wo')
        plot(t,Ttheory,'w')
end
plot(t(points),T(points),'wo')
% grid
ylabel('Temperature [K]')
hold

subplot(2,1,2)
plot(t,h,'w')
hold
if wetrun == 'y';
        plot(t(t_start),hwet,'wo')
        plot(t(t_stop),hwet,'wo')
        plot(t(t_stop),hdry,'wo')
else
        plot(t(t_start),hdry,'wo')
end
plot(t(points),hdry,'wo')
% grid
xlabel('Time [s]')
ylabel('h [W/m^2/K]')
hold


end
```

% tester.m

% This program generates a theoretical surface temperature
% history for a semi-infinite solid exposed to surface
% convection. See equation 5.60, Incropera and DeWitt.

% The generated temperature history is then used to test
% the algorithm used to back out the convection coefficient,
% h(t). If the algorithm works properly, it will return
% the same h that was input to generate the temperature
% history.

% The algorithm below labeled "Back out h(t)" is identical
% to that used in the program "convec," which is used to
% determine h(t) from actual temperature history data files.

% ----------------- CLEAR ALL VARIABLES --------------------

```
check = input('Do you wish to CLEAR? (y/n) ','s');
if check == 'y';
        clear
end
```

% ---------------- SUBSTRATE PROPERTIES --------------------

% Properties of Chromel at 300 K. Chromel is the material that
% makes up the tube of the coaxial thermocouples:
% Provided by the manufacturer, Medtherm Corp.


```
rho = 8730.;            % [kg/m^3]
c = 426.4;              % [J/kg/K]
k = 17.3;               % [W/m/K]

alpha = k/rho/c;  % [m^2/s]

rck = rho*c*k;
```

% ------- GENERATE TEMPERATURE HISTORY AT TC STA 1 ----------

```
Ti = 303.;              % Initial wall surface temp [K]
h = 10000.;             % Convection coefficient [W/m^2/K]
Taw = 1200.;            % Adiabatic wall temp [K]

t(1)=0;
T(1)=Ti;
for j = 2:2000;
        t(j) = t(j-1) + 0.000001;
        rhs1 = h * sqrt(alpha*t(j)) / k;
        rhs = 1 - exp(rhs1^2) * erfc(rhs1);
        T(j) = (Taw - Ti) * rhs + Ti;
end
```

72

```
t = t';            % Convert row to a column vector
T = T';            % Convert row to a column vector

% ------------------- BACK OUT h(t) -------------------------

h(1) = 0.;
for J = 2:2000;
        sum = 0.0;
        for j = 2:J;
                term = (T(j)-T(j-1)) / .....
                        (sqrt(t(J)-t(j))+sqrt(t(J)-t(j-1)));
                sum = sum + term;
        end
        q = 2. * sqrt(rck/pi) * sum;
        h(J) = q / (Taw - T(J));
end

h = h';            % Convert row to a column vector

% ------------------- PLOTS --------------------------------

figure(1)
subplot(2,1,1)
plot(t,T,'g')
title('"tester" results')
ylabel('Temperature [K]')

subplot(2,1,2)
plot(t,h,'b')
xlabel('Time [s]')
ylabel('h [W/m^2/K]')


end
```

Appendix C - Uncertainty Analysis

Uncertainties propagated through equations as follows:

For the equation $R = ab + c$,

$$\Delta R = \left[\left(\frac{\partial a}{\partial R} \Delta a \right)^2 + \left(\frac{\partial b}{\partial R} \Delta b \right)^2 + \left(\frac{\partial c}{\partial R} \Delta c \right) \right]^{1/2}$$

where Δa represents the uncertainty associated with the variable a. In some cases, the result of this relation can be simplified by dividing by the original equation to obtain $\Delta R/R$.

Four primary sources of uncertainty were identified and considered in the determination of the uncertainty of h and η. They are:

1. *Radiation.* The emissivity, ϵ, of the porous material is unknown. An analysis of radiation was performed assuming $\epsilon = 1$, the maximum possible value. This analysis showed the heat flux due to radiation to be just under 7% of the total heat flux for all conditions tested. Because of this, the calculated values of h are high by some unknown amount, not more than 7%. This uncertainty is reflected in the "-" portion of the uncertainty in Figs 4.2, 4.4, and 4.5. However, in calculating η, h_c is normalized to h_u. The radiation is assumed to be consistent in the cooled and uncooled conditions, and therefore the uncertainty due to radiation is not considered in finding the uncertainty in η.

2. *Stagnation Pressure.* P_o increased linearly throughout the steady state period due to shock attenuation. The variation in P_o was 10-15%. This uncertainty propagates to an uncertainty in T_{aw} as follows:

From Eq (2.17),

$$\Delta T_o = \frac{T_5}{P_5} \Delta P_o$$

Where ΔT_5 and ΔP_5 are assumed small relative to ΔP_o and are therefore

neglected. Then from Eq (2.19),

$$\Delta T_g = \left(1 + \frac{\gamma - 1}{2} M^2\right)^{-1} \Delta T_o$$

Finally, from Eq (2.21),

$$\Delta T_{aw} = \left(1 + \frac{r(\gamma - 1)}{2} M^2\right) \Delta T_g$$

Note that the uncertainty in M due to the resolution of the caliper used to measure

the nozzle dimensions was calculated and found to be negligible relative to the other

sources of uncertainty considered.

3. *Measured Wall Surface Temperature.* The coaxial thermocouples have an advertised

accuracy of ± 1 K. A simple statistical analysis was performed on 5,000

measurements of the wall surface temperature under static conditions. This analysis

confirmed ± 1 K to be one standard deviation. In the data filtering process, each

temperature measurement was averaged with the 25 previous points and 25

following points. Throughout this time period (51 μs), the change in measured

temperature was always very small, so the uncertainty in the temperature

measurement was improved by the filter as

$$\Delta T_{filtered} = \frac{\Delta T_{measured}}{\sqrt{\#points}} = \frac{1K}{\sqrt{51}} = 0.14K$$

This uncertainty propagates through Eq (2.1) in the determination of the total heat

flux. For each time step, the incremental temperature change must be summed from

$t = 0$ to the time step in question. It is unclear how the uncertainty would propagate through this summation (of up to 1,500 terms). Several derivations were attempted, with no reasonable result. Kline and McClintock (1953:6) state the uncertainty resulting from the summation of an infinite number of variables will not exceed 15%. This value was then taken as a conservative estimate of the uncertainty due to this summation, represented as

$$\left(\frac{\Delta q''}{q''}\right)_\Sigma = 0.15$$

Note that the values of ρ, c, and k in Eq (2.1) are considered to be well determined, and are not considered as significant sources of uncertainty in q". So for dry runs, the uncertainty in the calculated total heat flux is

$$\left(\frac{\Delta q''}{q''}\right)_{(uncooled)} = \left(\frac{\Delta q''}{q''}\right)_\Sigma = 0.15$$

4. *Nozzle wetting procedure.* The repeatability of the procedure used to wet the nozzle is questionable. This is expected to affect the starting location of the gas-liquid interface shown in Fig 2.1. It is unknown whether this will significantly impact the effectiveness of the cooling or just the duration of the cooling before dryout. To be conservative, this questionable wetting procedure is taken to introduce a 20% uncertainty in the calculated total heat flux. This is represented as

$$\left(\frac{\Delta q''}{q''}\right)_{wetting} = 0.20$$

So for wet runs, this effect must be considered along with $\Delta q''_\Sigma$.

$$\left(\frac{\Delta q''}{q''}\right)_{(cooled)} = \sqrt{\left(\frac{\Delta q''}{q''}\right)_\Sigma^2 + \left(\frac{\Delta q''}{q''}\right)_{wetting}^2} = 0.25$$

The sources of uncertainty discussed above combined as follows to create uncertainty in h.

From Eq (2.3),

$$\frac{\Delta h}{h} = \left[\left(\frac{\Delta q''}{q''} \right)^2 + \frac{\Delta T_{aw}^2 + \Delta T_w^2}{(T_{aw} - T_w)^2} \right]^{1/2}$$

And then the uncertainty of η from Eq (4.4) is given by

$$\Delta \eta = \left[\left(-\frac{100}{h_u} \Delta h_c \right)^2 + \left(\frac{100 h_c}{h_u^2} \Delta h_u \right)^2 \right]^{1/2}$$

Bibliography

Anderson, John D. Jr. <u>Modern Compressible Flow</u> (2nd Edition). McGraw-Hill Publishing Company, 1990.

Bowman, W.J., M.E. Himes, R.J. McMullan, R.C. Wier, and M.P. Wilson. "A Review of Transpiration Cooling in Pipes," AIAA 97-2575, <u>Proceedings of the 32nd AIAA Thermophysics Conference</u>, June 1997.

Chadwick, K.M. "Stagnation Heat Transfer Measurement Techniques in Hypersonic Shock Tunnel Flows over Spherical Segments," AIAA 97-2493, <u>Proceedings of the 32nd AIAA Thermophysics Conference</u>, June 1997.

Chen, Fu-Jung <u>Effects of Blowing Ratios on Heat Transfer to the Throat Region of a Porous-Walled Nozzle</u>. Masters Thesis, AFIT/GAE/ENY/95J-01. School of Engineering, Air Force Institute of Technology, Wright Patterson AFB OH, June 1995.

Choi, S.H., S.J. Scotti, K.D. Song, and H.R. Ries. "Transpiration Cooling of a Scram-Jet Engine Combustion Chamber," AIAA 97-2576, <u>Proceedings of the 32nd AIAA Thermophysics Conference</u>, June 1997.

Hazelton, David M. <u>Direct Measurement of Skin Friction in High Temperature and Impulsively Started Supersonic Flowfields</u>. Doctoral Dissertation, AFIT/DS/ENY/96-9. School of Engineering, Air Force Institute of Technology, Wright Patterson AFB OH, June 1996.

Hill, Philip G and Carl R. Peterson. <u>Mechanics and Thermodynamics of Propulsion</u> (2nd Edition). New York: Addison-Wesley Publishing Company, 1992.

Incropera, Frank P. and David P. DeWitt. <u>Fundamentals of Heat and Mass Transfer</u> (4th Edition). New York: John Wiley & Sons, Inc., 1996.

Kacynski, K.J. and J.D. Hoffman. "The Prediction of Nozzle Performance and Heat Transfer in Hydrogen/Oxygen Rocket Engines with Transpiration Cooling, Film Cooling, and High Area Ratios," AIAA 94-2757, <u>Proceedings of the 30th AIAA/SAE/ASME/ASEE Joint Propulsion Conference</u>, June 1994.

Kendall, David N. and W. Paul Dixon. "Heat Transfer Measurements in a Hot Shot Wind Tunnel," McDonnell Aircraft Corporation, St. Louis MO, July 1966.

Keenan, J.H., J. Chao, and J. Kaye. <u>Gas Tables</u>. New York: John Wiley & Sons, 1983: 24.

Keener, David N. <u>Investigation of Boundary Layer and Performance Effects of Transpiration Cooling Through a Porous Plate in a Rocket Nozzle</u>. Masters Thesis, AFIT/GA/ENY/94D-3. School of Engineering, Air Force Institute of Technology, Wright Patterson AFB OH, December 1994.

Kline, S.J. and F.A. McClintock. "Describing Uncertainties in Single-Sample Experiments," Mechanical Engineering, Jan 1953.

Landis, Jay A. Numerical Study of a Transpiration Cooled Rocket Nozzle. Masters Thesis, AFIT/GA/ENY/95D-01. School of Engineering, Air Force Institute of Technology, Wright Patterson AFB OH, December 1995.

Lenertz, Joseph L. Effects of Blowing Ratio on Heat Transfer to the Throat Region of a Porous-Walled Nozzle. Masters Thesis, AFIT/GA/ENY/94D-7. School of Engineering, Air Force Institute of Technology, Wright Patterson AFB OH, December 1994.

Lezuo, M. and O.J. Haidn. "Transpiration Cooling in H2/O2-Combustion Devices," AIAA 96-2581, Proceedings of the 32nd AIAA/ASME/SAE/ASEE Joint Propulsion Conference, July 1996.

Medtherm Corporation. "Approximate Thermal Properties for Chromel P," Huntsville, AL. Personal Correspondence, August 1997.

Omega Engineering, Inc. Thermocouple Reference Tables, 1993: A7-A8:B70-B86.

Raghuraman, P., B.J. Anderson, S.N. Sieger, D.C. Rousar, J.W. Hidahl, K.E. Baxter. "The HEDI Transpiration Cooling Concept – Lightweight, Durable, Flight Proven," AIAA 94-2005, Proceedings of the 6th AIAA/ASME Joint Thermophysics and Heat Transfer Conference, June 1994.

Ren, F., J.R. Tang, Z.Z. Wu, L.Y. Liu, and H.S. Sun. "Influence of Transpiration Cooling on Laminar Boundary Layer Structure," AIAA 97-2578, Proceedings of the 32nd AIAA Thermophysics Conference, June 1997.

Sreekanth, S. and N.M. Reddy, "Correlations for Injection Cooled Surface Temperatures in Compressible High Speed Flows," AIAA 97-2577, Proceedings of the 32nd AIAA Thermophysics Conference, June 1997.

Sutton, George P. Rocket Propulsion Elements (Sixth Edition). New York: John Wiley and Sons, Inc., 1992.

Vlcek, Kevin M. An Investigation of the AFIT 2-Inch Shock Tube as a Flow Source for Supersonic Testing. Masters Thesis, AFIT/GA/ENY/94D-1. School of Engineering, Air Force Institute of Technology, Wright Patterson AFB OH, December 1994.

Vita

Capt Daniel J. Schieb was born on 11 May 1971 in East Cleveland, Ohio. He graduated from Ontario High School in 1989 and then from the University of Southern California in 1993. He graduated Cum Laude with a Bachelor of Science in Aerospace engineering and was commissioned through ROTC.

His first assignment was at Tyndall AFB, Florida where he served as an aircraft maintenance officer as part of the Operational Experience program for engineers. While at Tyndall, he married the former Mary Ellen Yost. He entered the Air Force Institute of Technology School of Engineering in May 1996.

REPORT DOCUMENTATION PAGE

Form Approved
OMB No. 0704-0188

Public reporting burden for this collection of information is estimated to average 1 hour per response, including the time for reviewing instructions, searching existing data sources, gathering and maintaining the data needed, and completing and reviewing the collection of information. Send comments regarding this burden estimate or any other aspect of this collection of information, including suggestions for reducing this burden, to Washington Headquarters Services, Directorate for Information Operations and Reports, 1215 Jefferson Davis Highway, Suite 1204, Arlington, VA 22202-4302, and to the Office of Management and Budget, Paperwork Reduction Project (0704-0188), Washington, DC 20503.

1. AGENCY USE ONLY *(Leave blank)*	2. REPORT DATE December 1997	3. REPORT TYPE AND DATES COVERED Master's Thesis

4. TITLE AND SUBTITLE

EFFECTS OF LIQUID TRANSPIRATION COOLING ON HEAT TRANSFER TO THE DIVERGING REGION OF A POROUS-WALLED NOZZLE

5. FUNDING NUMBERS

6. AUTHOR(S)

Daniel J. Schieb, Capt, USAF

7. PERFORMING ORGANIZATION NAME(S) AND ADDRESS(ES)

Air Force Institute of Technology
2750 P Street
WPAFB OH 45433-6583

8. PERFORMING ORGANIZATION REPORT NUMBER

AFIT/GA/ENY/97D-04

9. SPONSORING / MONITORING AGENCY NAME(S) AND ADDRESS(ES)

Phillips Laboratory/Propulsion Directorate
Edwards AFB, CA

10. SPONSORING / MONITORING AGENCY REPORT NUMBER

11. SUPPLEMENTARY NOTES

12a. DISTRIBUTION / AVAILABILITY STATEMENT

Approved for public release; distribution unlimited

12b. DISTRIBUTION CODE

13. ABSTRACT *(Maximum 200 words)*

This research effort investigated the effects of evaporation of water on the heat transferred to the wall of the diverging portion of a porous walled nozzle. The AFIT High Pressure Shock Tube was used with a two-dimensional Mach 3 nozzle. One flat surface of the nozzle was fitted with a layer of porous stainless steel from the nozzle throat to the exit. This porous material was saturated with water to simulate liquid transpiration cooling. Surface temperature data was taken in this region using fast-response coaxial thermocouples. Heat transfer was determined from the surface temperature history. Data was taken for stagnation pressures ranging from 2.0 to 5.2 MPa. The effectiveness of the cooling diminished with increasing stagnation conditions. Reduction in convection heat transfer coefficient ranged from 10% at higher stagnation pressures to 130% at the lowest stagnation pressure tested.

14. SUBJECT TERMS

Transpiration Cooling, Sweat Cooling, Rocket Nozzles, Porous Materials, Shock Tube, Heat Transfer

15. NUMBER OF PAGES
93

16. PRICE CODE

17. SECURITY CLASSIFICATION OF REPORT Unclassified	18. SECURITY CLASSIFICATION OF THIS PAGE Unclassified	19. SECURITY CLASSIFICATION OF ABSTRACT Unclassified	20. LIMITATION OF ABSTRACT UL

NSN 7540-01-280-5500

Standard Form 298 (Rev. 2-89)
Prescribed by ANSI Std. Z39-18
298-102